Autophagosomes fuse to phagosomes and play important roles in the degradation of apoptotic cells in *Caenorhabditis elegans*

Omar Peña-Ramos[1], Lucia Chiao[1], Xianghua Liu[1,2], Tianyou Yao[1], Henry He[1,3], and Zheng Zhou[1,4]

[1] Verna and Marrs McLean Department of Biochemistry and Molecular Biology, Baylor College of Medicine, Houston, TX 77030
[2] Current address: Caris Life Sciences, Inc., Tempe, AZ 85281
[3] Current address: Department of Neurology Resident Program, University of Texas Southwestern Medical Center, Dallas, TX 75390
[4] Corresponding author, zhengz@bcm.tmc.edu, 713-798-6489

Abstract

Autophagosomes are double-membrane intracellular vesicles that degrade protein aggregates, intracellular organelles, and other cellular components. In the nematode *Caenorhabditis elegans*, 113 somatic cells undergo apoptosis during embryogenesis and are engulfed and degraded by their neighboring cells. We discovered a novel role of autophagosomes in facilitating the degradation of apoptotic cells in *C. elegans* embryos using a real-time imaging technique. Specifically, double-membrane autophagosomes in engulfing cells are recruited to the surfaces of phagosomes containing apoptotic cells and subsequently fuse to phagosomes, allowing the inner membrane to enter the phagosomal lumen. Mutants defective in the production of autophagosomes display significant delays in the degradation of apoptotic cells, demonstrating the important contribution of autophagosomes to this process. The signaling pathway led by the phagocytic receptor CED-1, CED-1's adaptor CED-6, and the large GTPase dynamin (DYN-1) promote the recruitment of autophagosomes to phagosomes. Moreover, the subsequent fusion of autophagosomes with phagosomes requires the functions of the small GTPase RAB-7 and the HOPS complex. Our findings reveal that, unlike the single-membrane, LC3-associated phagocytosis (LAP) vesicles reported for mammalian phagocytes, canonical autophagosomes function in the clearance of *C. elegans* apoptotic cells. These findings add autophagosomes to the collection of intracellular organelles that contribute to phagosome maturation, identify novel crosstalk between the autophagy and phagosome maturation pathways, and discover the upstream factors that initiate this crosstalk.

Introduction

During metazoan development and adulthood, a large number of cells undergo apoptosis or cell suicide; these dying cells are engulfed by phagocytes and degraded inside phagosomes, vacuoles composed of the lipid bilayers originated from the plasma membrane [1,2]. Swift engulfment and degradation of apoptotic cells are critical for tissue remodeling, resolution of the wound area, prevention, and suppression of harmful inflammatory and autoimmune responses induced by the dying cells [2]. Critical to the degradation of phagosomal contents is the fusion of intracellular organelles, including lysosomes and early endosomes, to phagosomes, which results in the delivery of the content of these organelles to the phagosomal lumen [3]. Lysosomes are the most pivotal organelles to support phagosomal degradation. They contribute many kinds of hydrolytic enzymes, including proteases, nucleases, lipases, and hydrolyzing enzymes for polysaccharides to

the lumen of phagosomes [3]. The fusion of lysosomes to phagosomes also helps acidify the phagosomal lumen, creating a low pH condition in which the digestive enzymes are active [3]. Besides lysosomes and endosomes, whether other kinds of intracellular organelles fuse to phagosomes and contribute to the degradation of the apoptotic cells inside remains unknown.

Mammalian microtubule-associated protein 1 light chain 3 (MAP1-LC3, or LC3) protein is a member of the ATG8 protein family [4]. LC3 molecules that are conjugated to the lipid phosphatidylethanolamine (PE) are most often observed on the surfaces of autophagosomes, a kind of double-membrane organelles that is a key structure of macroautophagy [4]. In fact, LC3 is a well-established marker for autophagosomes [4]. In mammalian cells, lipidated LC3 molecules were also reported to label a novel kind of vesicles referred to as LC3-associated phagocytosis (LAP) vesicles, which are single-membrane vesicles [5]. LAP vesicles were reported to fuse to phagosomes and facilitate the degradation of apoptotic cells in mice [6-8].

Autophagy is an evolutionarily conserved cellular event that plays an essential role in maintaining cellular homeostasis by enveloping harmful protein aggregates and damaged cellular organelles in double-membrane autophagosomes and subsequently degrading them via fusion with lysosomes [9]. Autophagy also supports cell survival during nutrient starvation by capturing intracellular organelles into autophagosomes and converting them to nutrients and energy sources [9]. Autophagosome formation requires the organized action of a set of proteins known as **a**u**t**opha**g**ic related (ATG) proteins. It is a process of three sequential steps: initiation, nucleation, and expansion, until an autophagosome fully forms and closes [10]. After formation, autophagosomes undergo a maturation process through fusion with lysosomes, which provide digestive enzymes to degrade autophagosomal contents [10]. In the nematode *C. elegans*, several autophagy genes have been reported to facilitate the clearance of apoptotic cells [11-13]. However, it is unknown whether autophagosome, as a particular type of cellular organelle, is involved in the clearance of apoptotic cells or whether these *atg* genes have additional functions, such as forming LAP vesicles.

Although both are labeled with LC3, mammalian LAP vesicles and autophagosomes are different in several key aspects. First, LAP vesicles are single-membrane vesicles, unlike autophagosomes, which are double-membrane vesicles [5,10]. In addition, although the formation of LAP vesicles relies on a lot of autophagy genes, ulk1, atg13, and atg14, three genes whose product act in the initiation complex for autophagosomes, are dispensable for the generation of LAP vesicles [5,7,14]. During the initiation of autophagosomes formation, which starts with the appearance of a membrane structure known as a phagophore, ULK1, a serine-threonine kinase, forms a protein complex with ATG13 and two other proteins and phosphorylates the class-III phosphoinositide 3-kinase (PI3K) Vps34 as well as the rest of the Vps34 complex (Atg6, Atg14, and Vps15), triggering the production of PtdIns(3)P on the phagosphore [10]. These distinct features of autophagosomes and LAP vesicles distinguish whether an LC3-labeled vesicle is an autophagosome or a LAP vesicle.

During *C. elegans* embryonic development, 131 somatic cells undergo apoptosis and are swiftly engulfed and degraded by neighboring cells [15,16]. Apoptotic cells display a “button-like” structure under Differential Contrast Interference (DIC) microscopy and are referred to as cell corpses [15,16]. Mutants defective in the clearance of cell corpses exhibit an increased number of persistent cell corpses, a phenotype known as **ce**ll **d**eath abnormal (Ced) [17]. Previous genetic studies revealed two parallel, partially redundant pathways that primarily drive the clearance of *C. elegans* cell corpses. These include a signaling pathway led by CED-1, a phagocytic receptor, CED-6, an adaptor protein for CED-1, and DYN-1, a large GTPase playing many roles in membrane trafficking, and the other led by the small Rac1 GTPase CED-10, and CED-5 and

CED-12, the bipartite nucleotide exchange factor for CED-10 [18]. Unlike the CED-10 pathway, which primarily promotes cell corpse engulfment, the CED-1 pathway regulates both the engulfment and degradation of cell corpses [19]. CED-1 on neighboring engulfing cells recognizes the "eat me" signal on the surfaces of cell corpses and is enriched to the side of the plasma membrane facing a cell corpse [20]. This enrichment initiates the extension of pseudopods along the cell corpse and the subsequent closure of the phagocytic cup to form a nascent phagosome [21,22]. Moreover, CED-1 also plays a distinct role in initiating the degradation of phagosomal contents [19]. CED-1 remains transiently enriched on the surface of nascent phagosomes, where it facilitates the CED-6 and DYN-1-mediated sequential recruitment of the Class II phosphatidylinositol 3-bisphosphate (PtdIns(3)P) kinase PIKI-1, the Class III PtdIns(3)P kinase VPS-34, and the small GTPases RAB-5 and RAB-7 to phagosomal surfaces [19,23]. The robustly produced PtdIns(3)P and the RAB-5 and -7 GTPases further recruit PtdIns(3)P-binding proteins and effectors for the RAB proteins, respectively, which drive the recruitment and fusion of early endosomes and lysosomes to a phagosome, leading to the degradation of the cell corpse inside the phagosome [23-25]. RAB-7, in particular, is responsible for the fusion of lysosomes to phagosomes [19].

Autophagy and phagocytosis are two distinct lysosomal-mediated cellular degradation pathways designated to eliminate intracellular and extracellular components, respectively. Previously, whether canonical autophagosomes were involved in the degradation of phagosomal contents was unknown. We report here that, during the maturation of phagosomes that contain apoptotic cells in *C. elegans* embryos, LC3-labeled, double-membrane canonical autophagosomes are recruited to phagosomal surfaces and subsequently fuse to these phagosomes. Additionally, we have discovered that this event facilitates the degradation of apoptotic cells inside the phagosomal lumen and is driven by the signaling pathway led by CED-1. This autophagosome-phagosome fusion represents a novel mechanism that contributes to the degradation of phagosomal contents.

Results

Vesicles labeled with GFP-tagged LC3 are recruited to the surfaces of phagosomes

The ATG8 protein family is composed of two subfamilies, the LC3 subfamily, and the GABARAP subfamily, which are very close to each other in sequence; the ATG8 family is also referred to as the LC3/GABARAP family [4]. *C. elegans* has two LC3/GABARAP family members, LGG-1 and LGG-2, which belong to the LC3 and GABARAP subfamilies, respectively (**Fig 1A**) [26]. Both LGG-1 and LGG-2 are attached to autophagosomes, except that they each label autophagosomes of different maturity [26].

To determine whether autophagosomes interact with phagosomes that contain apoptotic cells in *C. elegans* embryos, we constructed GFP-tagged LGG-1 and LGG-2 reporters that were expressed under the control of the *ced-1* promoter (P_{ced-1}), a well-documented engulfing cell-specific promoter [20,27]. In embryos, we observed numerous GFP::LGG-1$^+$ and GFP::LGG-2$^+$ puncta (**Figs 1**, **S1A, S2A**). Using our previously established time-lapse microscopy protocol [27], we observed the enrichment of GFP::LGG-1$^+$ and GFP-LGG-2$^+$ puncta to the surface of the phagosomes, including phagosomes containing apoptotic cells C1, C2, and C3 (**Fig 1 B, D, G**). These GFP-labeled puncta were observed on the surface of phagosomes but not inside the phagosomal lumen (**Fig 1 D**, **G**, top panels).

C. elegans LGG-1 and LGG-2 were both reported to specifically attach to autophagosomes through their lipid tails [26,28]. To verify that the observed GFP puncta are LGG-labeled lipid vesicles and not artifacts of protein aggregation, we tested two mutant constructs, GFP::LGG-1(G116A) and GFP::LGG-2(G130A), which bear mutations in the lipidation sites of the LGG proteins and are deficient for membrane targeting [26].

We found that both GFP::LGG-1(G116A) and GFP::LGG-2(G130A) display a diffuse cytosolic localization pattern **(Fig 1 D**, **G**, bottom panels**)**, in stark contrast to the punctate pattern presented by GFP::LGG-1 and GFP::LGG-2. This result indicates that GFP::LGG-1 and GFP::LGG-2 are membrane attached and thus label lipid vesicles.

The LGG-tagged puncta that fuse to phagosomes are double-membrane vesicles

The fluorophore within GFP is sensitive to acidic pH (pKa=6.0) [29], thus its signal diminishes when GFP is inside the acidic lumen of lysosomes and phagosomes. To further monitor the fate of the GFP-LGG$^+$ puncta after they are recruited to the surfaces of phagosomes, we replaced GFP with mCherry (pKa<4.5) or mNeonGreen (mNG) (pKa=5.1), both of which are more resistant than GFP to the acidic pH environment inside the lumen of organelles such as lysosomes and phagosomes [30,31], allowing fluorescence signal inside the phagosomal lumen to be detected. Co-expressed with the mCherry::LGG or mNG::LGG reporter are CED-1::GFP or PH(hPLCγ)::mRFP reporters, which were used in the time-lapse experiments as markers of extending pseudopods, allowing us to determine the moment when the pseudopods sealed up and a nascent phagosome was born (**Fig 1 E**, **F**, **H**, **I,** top panels). In time-lapse image series of the clearance of C1, C2, and C3, we found that like the GFP::LGG reporters, the mCherry::LGG and mNG::LGG reporters were enriched on the surfaces of phagosomes; however, unlike the GFP::LGG reporters, the mCherry and mNG tagged reporters subsequently entered phagosomal lumen (**Fig 1 E**, **F**, **H**, **I**). The fluorescence signal intensity increases over time with the continuous recruitment of the LGG$^+$ puncta on phagosomal surfaces over time (**Fig 1 E**, **F**, **H**, **I, Movie S1, S2,** and **S3**). We measured the intensity of the mCherry::LGG-1 and mCherry::LGG-2 signal in the center of the C3 phagosomes over time from the start of the phagosome (**Materials and Methods**) (**Fig 1C**) and observed over 10-fold increases of the signal intensity within 60 min (**Fig 1J**). The appearance of the membrane-attached mCherry::LGG and mNG::LGG signal in the phagosomal lumen indicates that the LGG$^+$ vesicles fuse with the phagosomal membrane (**Fig 1K**). They further suggest that these vesicles are composed of double membranes labeled with the LGG reporter molecules on both the outer and inner membranes (**Fig 1K**). If these LGG$^+$ vesicles were single-membrane, no membrane-attached LGG reporter would end up inside the phagosomal lumen because, as a result of fusion, the reporter molecules will be retained on the phagosomal membrane (**Fig 1K**). Indeed, when CTNS-1, a lysosomal membrane protein, is tagged with mRFP, which is acid-resistant (pKa=4.5 [30]), on its C-terminus, the lysosome-phagosome fusion event resulted in the incorporation of the mRFP signal to the phagosomal membrane; no mRFP signal is observed in the phagosomal lumen (**Fig S3A**) [19].

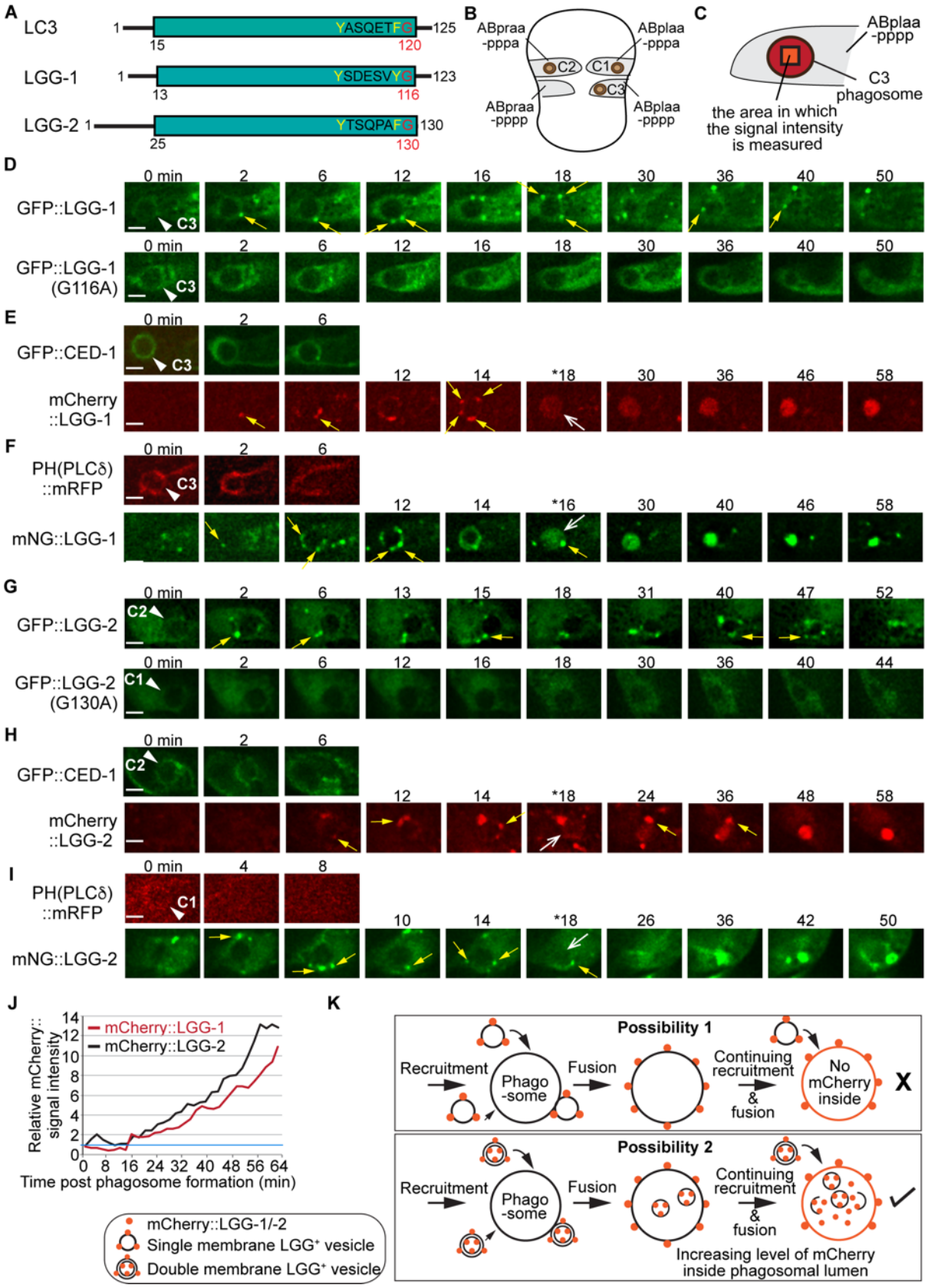
A
LC3
1
YASQETFG
125
15
120
LGG-1
1
YSDESVYG
123
13
116
LGG-2
1
YTSQPAFG
130
25
130
B
ABpraa -pppa
ABplaa -pppa
C2
C1
C3
ABpraa -pppp
ABplaa -pppp
C
ABplaa -pppp
C3 phagosome
the area in which the signal intensity is measured
D
GFP::LGG-1
GFP::LGG-1 (G116A)
0 min
2
6
12
16
18
30
36
40
50
C3
E
GFP::CED-1
mCherry ::LGG-1
0 min
2
6
12
14
*18
30
36
46
58
C3
F
PH(PLCδ) ::mRFP
mNG::LGG-1
0 min
2
6
12
14
*16
30
40
46
58
C3
G
GFP::LGG-2
GFP::LGG-2 (G130A)
0 min
2
6
13
15
18
31
40
47
52
12
16
30
36
44
C2
C1
H
GFP::CED-1
mCherry ::LGG-2
0 min
2
6
12
14
*18
24
36
48
58
C2
I
PH(PLCδ) ::mRFP
mNG::LGG-2
0 min
4
8
10
14
*18
26
36
42
50
C1
J
Relative mCherry:: signal intensity
mCherry::LGG-1
mCherry::LGG-2
0
2
4
6
8
10
12
14
0 8 16 24 32 40 48 56 64
Time post phagosome formation (min)
mCherry::LGG-1/-2
Single membrane LGG⁺ vesicle
Double membrane LGG⁺ vesicle
K
Possibility 1
Recruitment
Phago -some
Fusion
Continuing recruitment & fusion
No mCherry inside
X
Possibility 2
Recruitment
Phago -some
Fusion
Continuing recruitment & fusion
Increasing level of mCherry inside phagosomal lumen
✓

Figure 1. The vesicles labeled with LGG-1 or LGG-2 are recruited to the surface of phagosomes and subsequently fuse to phagosomes.

(A) Domain structures of mammalian LC3 and *C. elegans* LGG-1 and LGG-2. The green box indicates the conserved ubiquitin-like domain. Residues in white are conserved among the three proteins. The glycine residue in red is the site where the lipid tail is attached to.

(B) A diagram illustrating the three phagosomes that contain cell corpses C1, C2, and C3, with which we monitor the dynamic recruitment and fusion of autophagosomes, at ~330 min post-the 1st embryonic division. Both the positions of C1, C2, and C3 (brown dots) and the identities of their engulfing cells are shown.

(C) A diagram illustrating that the relative mNG signal in the center of a phagosome is measured over time to create sub-figure (J). At time point T (time after engulfment), the Relative signal intensity $_T$ = (Unit Intensity(phagosome center)$_T$ – Unit Intensity (background)$_T$) / (Unit Intensity(phagosome center)$_{T0}$ – Unit Intensity(background)$_{T0}$).

(D-I) Time-lapse images of indicated reporters starting when a nascent phagosome (white arrowheads) just formed (time point "0 min"). All reporters were expressed under the control of P_{ced-1}. Scale bars are 2 μm. Solid white arrowheads label nascent phagosomes. Yellow arrows mark a few LGG-labeled puncta on the surface of phagosomes. Open white arrows in (E, F, H, I) label the phagosomes when the LGG signal is first seen entered their lumen. "*" is the time point when the LGG signal is first seen inside the phagosomal lumen. CED-1::GFP (E, H) and PH(PLCγ)::mRFP (F, I) are co-expressed markers that label the surfaces of nascent phagosomes.

(D) GFP::LGG-1-labeled puncta are observed on the surface of a C3 phagosome, but the GFP signal is not seen inside the phagosomal lumen. No GFP::LGG-1(G116A)-labeled puncta are seen on the surface of phagosomes.

(E-F) The mCherry::LGG-1 (E) and mNG::LGG-1 (F) puncta are observed on the surface of a C3 phagosome and subsequently accumulate inside the phagosome lumen.

(G) GFP::LGG-2-labeled puncta are observed to attach on the surface of a C2 phagosome, but the GFP signal does not enter the phagosomal lumen, whereas no GFP::LGG-1(G130A)-labeled puncta are seen on the surface of phagosomes.

(H-I) The mCherry::LGG-2 (H) and mNG::LGG-2 (I) puncta are observed on the surface of a C2 (H) or C1 (I) phagosome, respectively, and subsequently accumulate inside the phagosome lumen.

(J) The relative mCherry::LGG-1 or -2 signal intensity in the center of a phagosome (Y-axis) over time (in 2-min interval) (X-axis). "0 min" indicates the moment when a nascent phagosome just formed. One blue horizontal line indicates value "1", where no signal enrichment above background level is observed.

(K) A diagram illustrating that those double membrane-vesicles labeled with mCherry::LGG on their outer and inner membranes are recruited to phagosomal surfaces and fused to the phagosomal membrane. After the fusion between the outer membrane of these vesicles and phagosomal membrane, the mCherry::LGG-tagged inner membrane enters the phagosomal lumen. The continuing incorporation of these double-membrane vesicles to phagosomes increases the mCherry signal level in the phagosomal lumen, observed over time. If the LGG-1 or LGG-2-labeled vesicles are of a single membrane, no fluorescence signal is expected to enter the phagosomal lumen.

The LGG$^+$ vesicles that are incorporated into phagosomes are canonical autophagosomes

The observation that the LGG$^+$ vesicles incorporating into phagosomes are likely composed of double membranes reminded us of canonical autophagosomes rather than LAP vesicles. To further determine whether

these vesicles represent autophagosomes, we examined whether loss-of-function mutations of *atg-7*, *atg-13*, and *epg-8*, which are defective for the biogenesis of autophagosomes [32,33], impair the production of these vesicles. *C. elegans atg-13* and *epg-8* encode homologs of mammalian Atg13 and Atg14, respectively, which are essential for the biogenesis of autophagosomes but not LAP vesicles (**Introduction**) [34]. *atg-7* encodes a homolog of mammalian Atg7, a protein essential for conjugating a phospholipid tail onto the LC3 family proteins [10,34]. We first scored whether the mCherry::LGG-1/-2 reporters were observed in the center of 15 phagosomes during the phagosome maturation process (**Figs 1C** and **2**), which is indicative of the fusion of mCherry::LGG $^{+}$ vesicles to phagosomes. In wild-type embryos, the steady entry of mCherry into phagosomes over time (**Fig 1 E**, **H**) results in the increase of the average mCherry::LGG-1 and -LGG-2 intensities to 9.2- and 8.4-fold of that at 0 min time point, respectively, at 60 min after the formation of a phagosome (**Fig 2 H**, **J**). However, in *atg-7(bp411)* [35] mutant embryos, hardly any mCherry signal was observed inside phagosomes **(Fig 2 A, D, G-J)**. At 60 min after phagosome formation, the average mCherry signal intensities were merely 1.2 and 1.4-fold at 0 min time point **(Fig 2 H, J).** These observations indicate a lack of LGG^{+} vesicles that fuse to phagosomes. In *atg-13(bp414)* and *epg-8(bp251)* mutant embryos, similar observations were made except that the defects were slightly weaker (**Fig 2 B, C, E, F, G-J**).

We further examined whether the mCherry::LGG-1/-2^{+} vesicles appeared in the *atg-7*, *atg-9*, *atg-13*, and *epg-8* mutant embryos. In wild-type embryos at mid-embryonic developmental stages (~330, ~350, ~400 min post-1st embryonic cell division), numerous mCherry^{+} puncta were observed (**Figs S1A, S2A**). In the *atg-7* mutant embryos, rarely any such puncta existed (**Figs S1B, S2B**), consistent with a previous report [32]. *atg-9* encodes ATG-9, the only transmembrane protein in the core autophagy machinery [32,34]. ATG9 plays an essential role in the expansion of phagophore and the biogenesis of autophagosomes [10]. In *atg-9(bp564)* mutant embryos that expressed mNG::LGG-1 or ::LGG-2, much fewer mNG^{+} puncta that might represent autophagosomes were observed, and the mNG reporters label large aggregates (**Fig S4**), consistent with a previous report [36]. The reduction in the number of LGG-1/-2-labeled puncta in *atg-7* and *atg-9* loss-of-function mutants indicates that these puncta belong to autophagosomes.

In *atg-13* and *epg-8* mutant embryos, the numbers of mCherry-LGG^{+} puncta were significantly reduced (**Figs S1 C-D, S2 C-D**), suggesting that the *atg-13(bp414)* and *epn-8(bp251)* mutations severely impaired the biogenesis of autophagosomes, a phenotype that is consistent with previous reports [32,33]. These phenotypes also support that the LGG^{+} puncta were canonical autophagosomes.

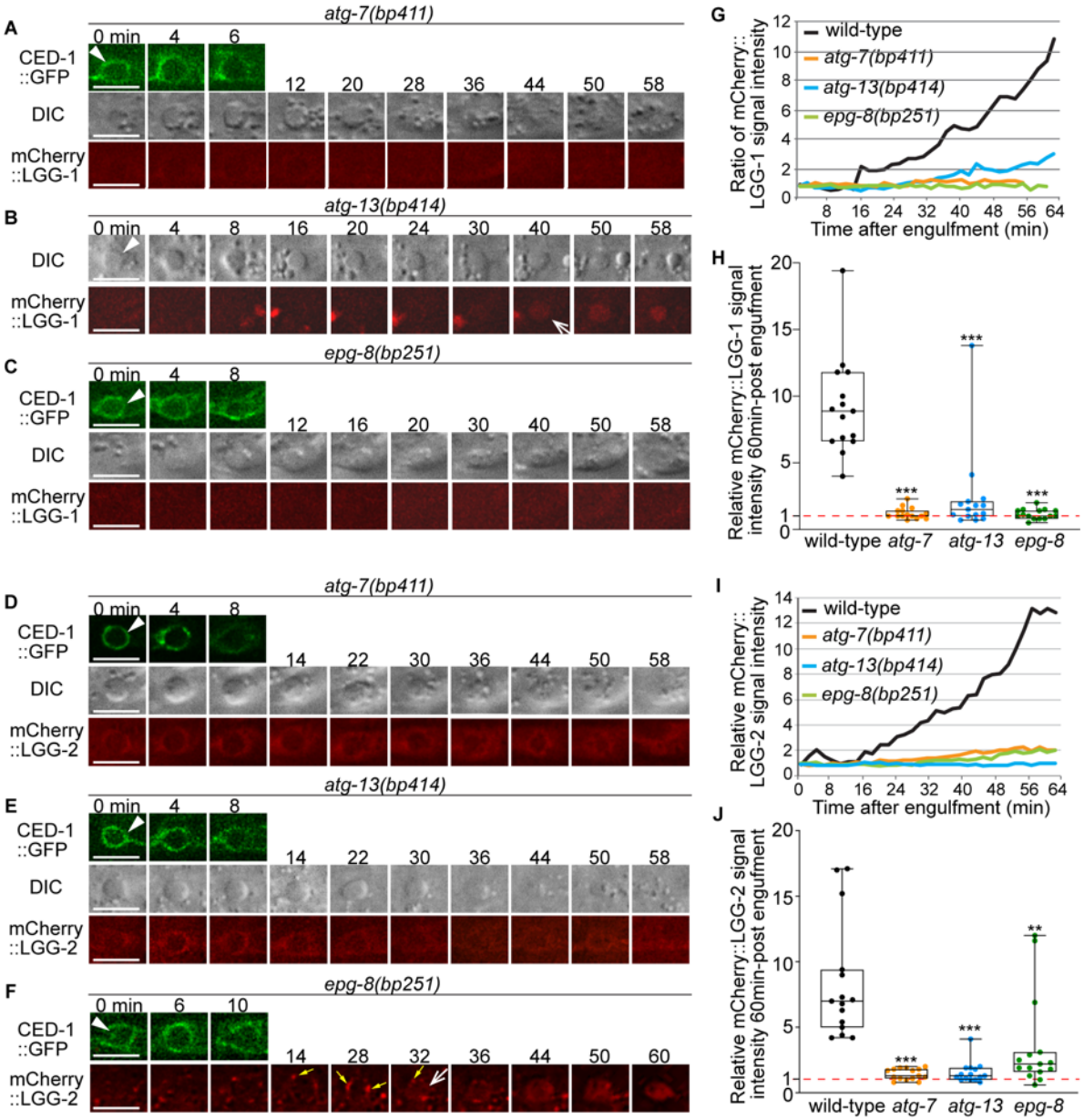

Figure 2. In autophagosome-formation mutants, the enrichment of the LGG⁺ vesicles on the phagosomal surface and the entry of the LGG signal into the phagosomal lumen are both severely defective.
(A-F) Time-lapse image series monitoring the enrichment of the puncta labeled with mCherry-tagged LGG-1 (A-C) or LGG-2 (D-F) on phagosomes (white arrowheads) and the subsequent entry of mCherry signal into the phagosomal lumen in *atg-7*, *atg-13*, and *epg-8* mutant embryos. DIC images mark the position of the cell corpse. "0 min" is when a phagosome is just sealed (determined by CED-1::GFP). "*" denotes the time point that the mCherry signal starts to appear inside the phagosomal lumen. Scale bars are 2μm. Yellow arrows in (F) mark mCherry::LGG-2 puncta on the surface of a phagosome (open white arrow).
(G and I) The relative mCherry::LGG-1 or -2 signal intensity in the center of a phagosome (Y-axis) over time (in 2-min interval) (X-axis). "0 min" indicates the moment when a phagosome is just sealed. (G) The data for the wild-type, *atg-7(bp411)*, *atg-13(bp414)*, and *epg-8(bp251)* mutant embryos are from Figures 1E and 2(A-

C), respectively. (I) The data for the wild-type, *atg-7(bp411)*, *atg-13(bp414)*, and *epg-8(bp251)* mutant embryos are from Figures 1I and 2(D-F), respectively.
(H and J) Box-and-Whiskers plots of the relative mCherry signal intensity measured in the center of phagosomes 60 min-post the formation of nascent C3 phagosomes from 15 each of wild-type, *atg-7(bp411)*, *atg-13(bp414)*, and *epg-8(bp251)* mutant embryos. Red dashed lines indicate the position of value 1, which represents no signal enrichment relative to the background signal.
***, $p<0.001$, **, $<0.001p<0.01$, Student *t*-test of each mutant comparing to the wild-type value.

To further confirm that autophagosomes fuse to phagosomes, we examined the subcellular localization of a mCherry::ATG-9 reporter expressed in engulfing cells. Besides the LGG proteins, ATG-9 is also an established autophagosomes marker as it is the only transmembrane protein in autophagosomes [37]. In embryonic hypodermal cells that co-expressed mCherry::ATG-9 and either mNG::LGG-1 or::LGG-2, puncta labeled with mCherry::ATG-9 are recruited to the surfaces of phagosomes (**Fig 3**). Furthermore, the mCherry signal gradually accumulates in the phagosomal lumen like the LGG reporters do (**Fig 3**). During the phagosome maturation process, co-localization between mCherry::ATG-9 and each of the two LGG reporters on the puncta on phagosomal surfaces and inside phagosomal lumen was nearly perfect (**Fig 3**). Together, the above observations verified that autophagosomes on which membranes ATG-9 and LGG proteins are present are recruited to phagosomal surfaces and subsequently fuse to phagosomes containing apoptotic cells.

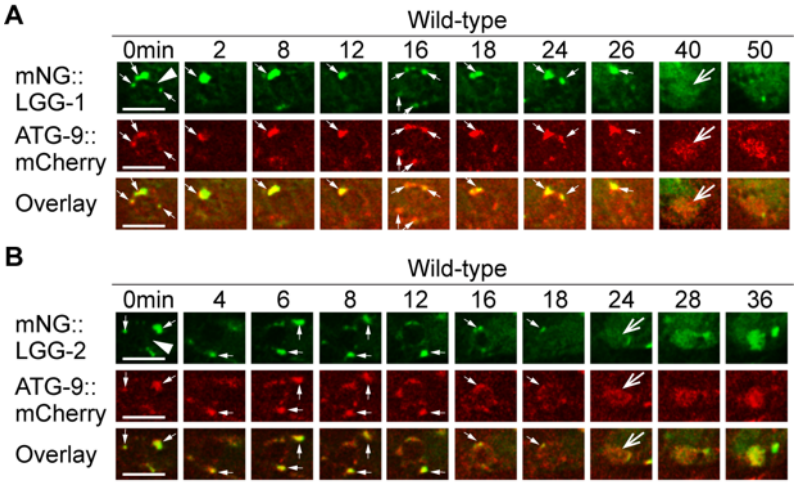

Figure 3. LGG-1 and LGG-2$^+$ puncta colocalize with ATG-9, a component of autophagosomes.
The mNG- and mCherry-tagged reporters are expressed in wild-type embryos under the control of P_{ced-1}. White arrowheads make nascent phagosomes. Small white arrows mark the regions where LGG$^+$ and ATG-9$^+$ puncta colocalize. Open white arrows indicate the moment when the fluorescent signal is first detected inside the phagosomal lumen. Scale bars are 5 μm.
(A) Time-lapse microscopy showing the localization of mNG::LGG-1 and mCherry::ATG-9. Images are from ABplaapppp, which engulfs C3.
(B) Time-lapse microscopy showing the localization of mNG::LGG-2 and mCherry::ATG-9. Images are from ABplaapppa, which engulfs C1.

Autophagosomes facilitate the degradation of apoptotic cells inside phagosomes

To examine whether the incorporation of autophagosomes into phagosomes affects the clearance of the engulfed apoptotic cells, we first quantified whether, in mutants of autophagy genes, apoptotic cells were un-degraded and persistent in embryos. In addition to the *atg-7*, *atg-9*, *atg-13*, and *epg-8* mutants characterized above, we also characterized loss-of-function mutants of *lgg-1* and *lgg-2*, and of *atg-3*, whose gene product is essential for the conjugation of a PE tail to the LC3 family proteins, like ATG-7 [32,38], of *atg-2* and *atg-18*, whose gene products function together with ATG-9 in the expansion of phagophore [37], and of *unc-51*, which encodes a *C. elegans* homolog of ULK1, an autophagic protein kinase [37]. In 2-fold stage wild-type embryos, which are ~460 min post the first embryonic cell division, an average of 11.3 cell corpses were scored (**Fig 4A**). The mutant 2-fold embryos examined bore 46.9% - 91.2% more cell corpses (**Fig 4)**, indicating that the clearance of cell corpses is defective. Together, the findings reported in **Figs 2**, **3**, and **4** indicate that autophagosomes made a substantial contribution to the clearance of cell corpses.

To determine whether the lack of autophagosomes impairs the engulfment or degradation of cell corpses, we monitored the formation and degradation of phagosomes engulfing ventral apoptotic cells C1, C2, and C3 (**Fig 1B**) in wild-type and *lgg* mutant embryos in real-time using established protocol **(Materials and Methods)** [24,27]. CED-1::GFP, which is expressed in engulfing cells under the control of P_{ced-1}, labels the extending pseudopods and enables us to monitor the process of phagosome formation, starting from the budding of and ending at the sealing of the pseudopods [20,21]. 2xFYVE::mRFP (also expressed under P_{ced-1}), a reporter for phagosomal surface PtdIns(3)P, enables us to monitor the shrinking of a phagosome, an indication of phagosome degradation [19,23,24]. In *atg-7*, *lgg-1,* and *lgg-2* mutant strains that co-expressed CED-1::GFP and 2xFYVE::mRFP, we found that engulfment was completed in 4-8 min, just like in wild-type embryos (**Fig 5 A-D**), indicating that defects in autophagosomes formation do not affect the engulfment of cell corpses. However, the lifespans of phagosomes (**Materials & Methods**) were much longer in *atg-7*, *lgg-1*, and *lgg-2* mutants than in wild-type embryos (**Fig 5**). All wild-type phagosomes have a lifespan between 40-60 min (**Fig 5F**). In *atg-7*, *lgg-1,* and *lgg-2* mutants, the lifespan varied in a much more extensive range. Remarkably, 43.8%, 53.3%, and 82.4% of phagosomes in *atg-7*, *lgg-2,* and *lgg-1* mutant embryos, respectively, have lifespans longer than 60 min (**Fig 5F**). The longest persisting phagosome, which was observed in an *lgg-1* mutant embryo, lasted longer than 136 min (**Fig 5D**). These observations indicate that autophagosomes made a significant contribution to the efficient degradation of phagosomal contents.

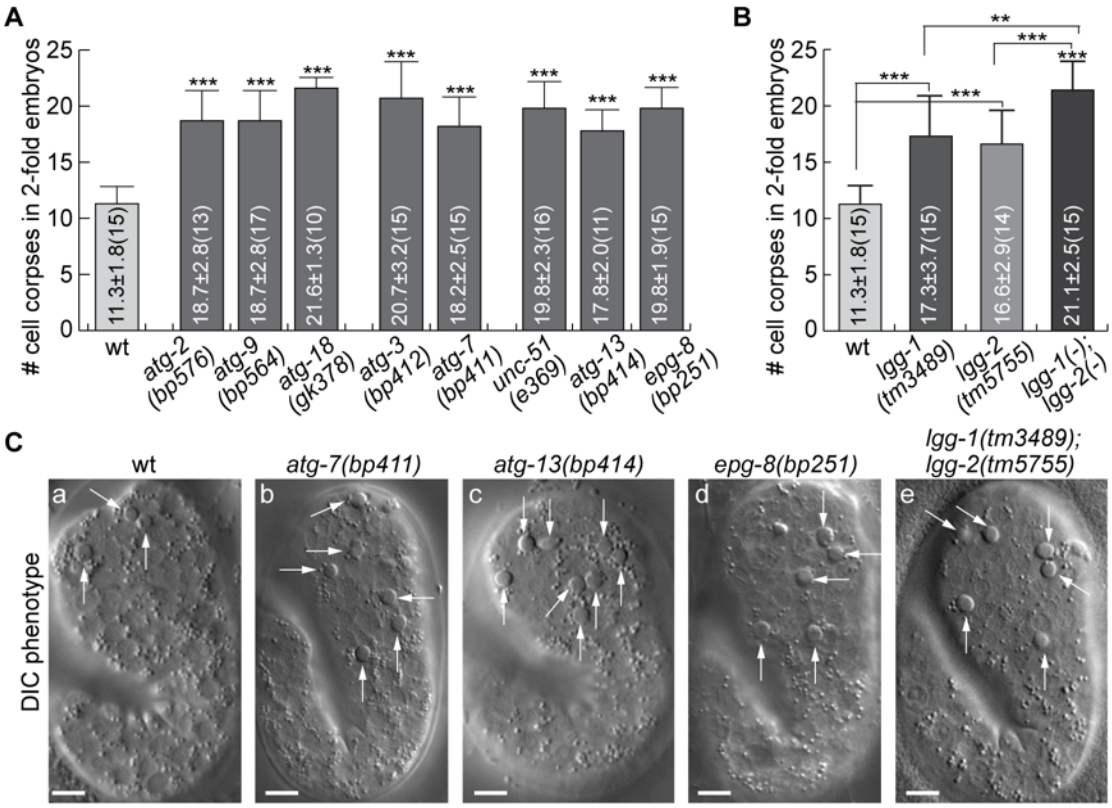

Figure 4. Mutations in autophagy genes impair the clearance of apoptotic cells.
(A-B) Bar graph displaying the average numbers of somatic cell corpses in 2-fold stage wild-type and various mutant embryos. Bars and error bars represent mean and standard deviation (sd), respectively, the actual values of which are displayed inside the bars. Numbers in parentheses indicate the number of embryos scored. ***, $p<0.001$, Student *t*-test of each mutant comparing to the wild-type value.
(C) DIC images of cell corpses in 2-fold stage embryos of various genotypes. White arrows indicate button-like structures characteristic of cell corpses. Scale bars are 5 μm.

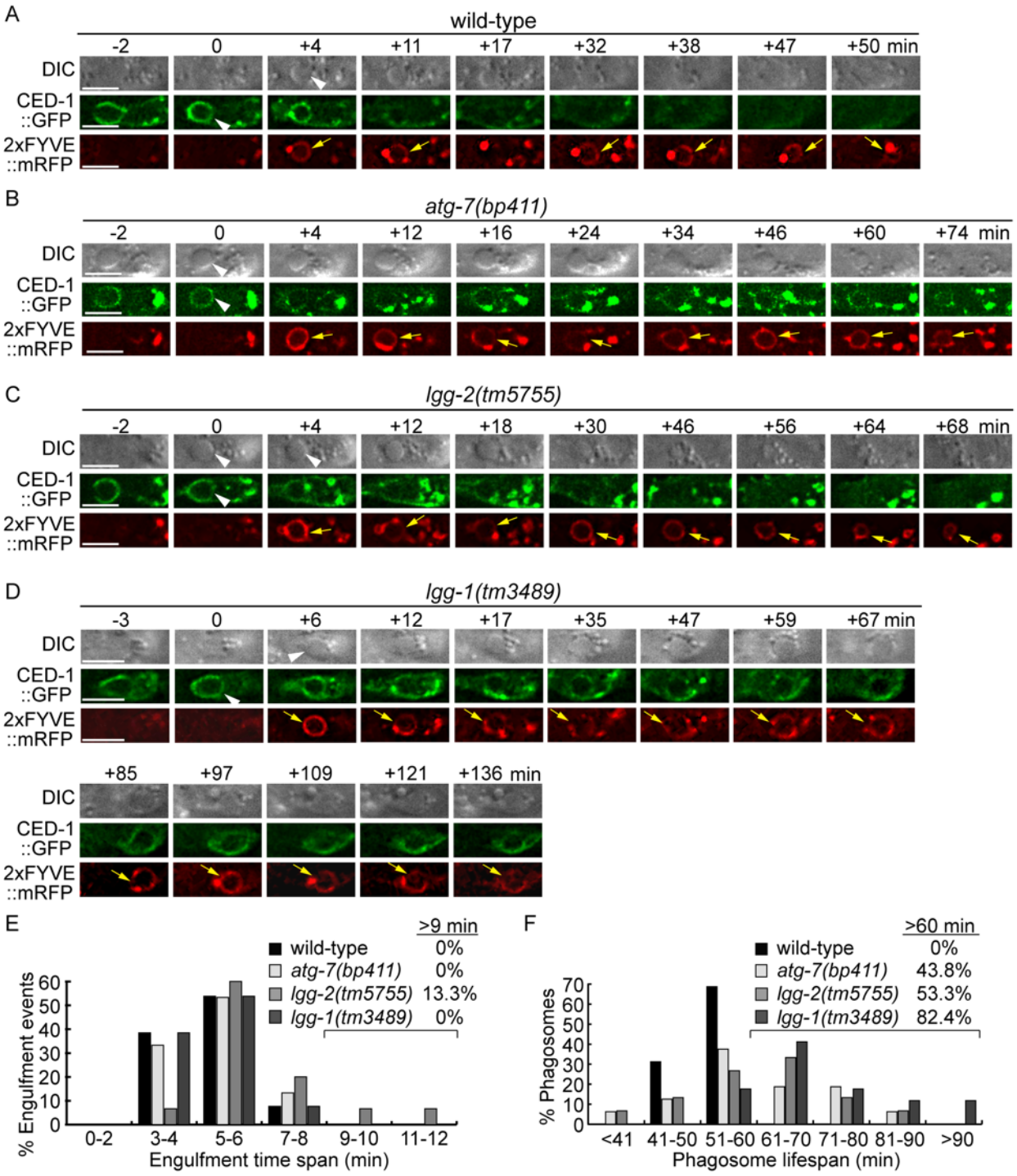

Figure 5. Mutations in *atg-7*, *lgg-1*, and *lgg-2* delay the degradation of cell corpses.
(A-D) Time-lapse recording conducted in wild-type and different mutant embryos monitoring the dynamics of the pseudopod marker CED-1::GFP and the phagosome marker 2xFYVE::mRFP (both expressed in engulfing cells) during the engulfment and degradation processes of cell corpse C3 by ABplaapppp. "0 min" is the first time point when a nascent phagosome (white arrowheads) is formed, as indicated by the closure of a green GFP::CED-1 ring. 2xFYVE::mRFP labels the surface of a phagosome (yellow arrows) until it is degraded. Scale bars are 2 μm.

(E) Histogram depicting the distribution of the time it takes to engulf 15 C3 cell corpses in each of the four genotypes. The engulfment time is defined as the period between the first time point when pseudopods (labeled with CED-1::GFP) are spotted and the time point when a full circle forms around C3.
(F) Histogram depicting the distribution of the duration of 15 C3 phagosomes in each of the four genotypes. Phagosome lifespan is measured as the time interval between the "0 min" time point and the time point when the phagosome shrinks to one-half of its original diameter.

LGG-1 and LGG-2 act in engulfing cells, and together they define three subpopulations of autophagosomes that are incorporated into phagosomes

LGG-1 and LGG-2 have distinct structural features and were observed to attach to different sub-populations of autophagosomes, which represent autophagosomes at different maturation stages [26,28]. The sub-populations of autophagosomes labeled by LGG-1- or LGG-2- are incorporated into phagosomes (**Fig 1**). *lgg-1* and *lgg-2* single mutant strains are both inefficient in clearing cell corpses (**Fig 4B**). Furthermore, in *lgg-1; lgg-2* double mutant embryos at 2-fold, the Ced phenotype is further enhanced significantly (**Fig 4B**) -- the number of cell corpses is 22.0% and 27.1% more than in the *lgg-1* and *lgg-2* single mutants, respectively. This enhanced phenotype indicates an additive effect and suggests that the autophagosomes labeled with LGG-1 or LGG-2 play parallel and partially redundant roles in promoting phagosome degradation. In embryos co-expressing mCherry::LGG-1 and mNG::LGG-2, we observed that in engulfing cells and on the surfaces of phagosomes, puncta were either labeled with mCherry or mNG alone and puncta that were labeled with both (**Fig 6**). This observation indicates that in addition to the LGG-1^{+}-only and LGG-2^{+}-only subpopulations, a third LGG-1^{+} LGG-2^{+} double-positive subpopulation of autophagosomes exists. This subpopulation likely corresponds to an intermediate stage during the maturation path of autophagosomes.

To determine whether LGG-1 and LGG-2 act in engulfing cells to facilitate phagosome degradation, we examined whether the specific expression of each gene in engulfing cells, under the control of P_{ced-1}, would rescue the Ced phenotype of the corresponding mutant embryos. We tested both the *gfp*- and *mCherry*-tagged *lgg* cDNAs for the rescuing activity by counting the number of cell corpses in 1.5-fold stage transgenic embryos. In the *lgg-1* and *lgg-2* null mutants, both the *gfp*- and *mCherry*-tagged corresponding *lgg* cDNA efficiently rescued the Ced phenotype (**Fig S5**). The *gfp::lgg-1* and *mCherry::lgg-1* transgenes lowered the number of cell corpses from on-average 152% of wild-type level observed in the *lgg-1(tm3489)* mutants to 118% and 123% of the wild-type level, respectively. Similarly, the *gfp::lgg-2* and *mCherry::lgg-2* transgenes lowered the number of cell corpses from on-average 143% of wild-type level observed in the *lgg-2(tm5755)* mutants to 109% and 112% of the wild-type level, respectively (**Fig S5**). These results indicate that *lgg-1* and *lgg-2* primarily act in engulfing cells to facilitate the clearance of apoptotic cells.

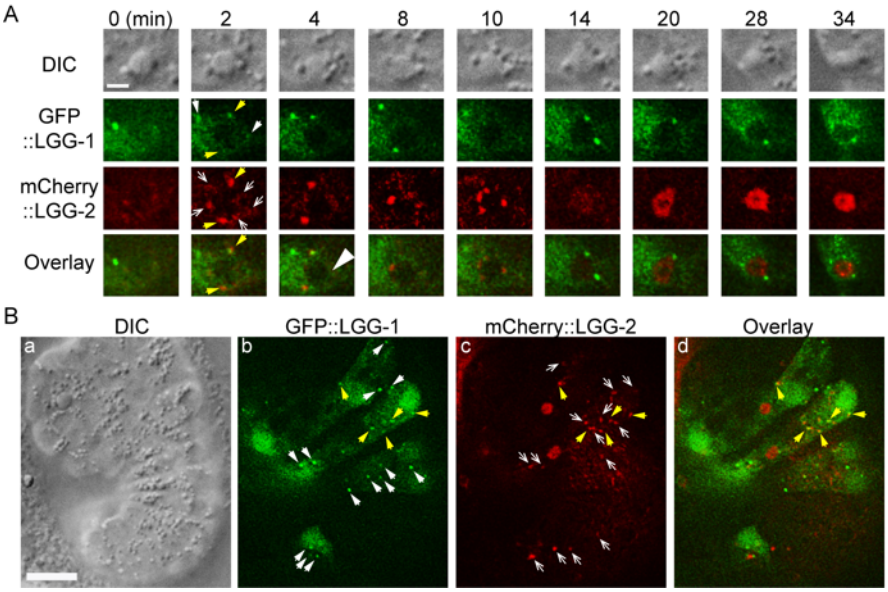

Figure 6. The puncta labeled with LGG-1 and/or LGG-2 define three distinct populations of vesicles
The time-lapse recording was conducted on wild-type embryos co-expressing P_{ced-1}*gfp::lgg-1* and P_{ced-1}*mCherry::lgg-2*.
(A) Time-lapse image series of a C2 phagosome (one big white arrowhead in the "4 min" image). "0 min" is the moment when a nascent phagosome just seals. The scale bar is 2 μm. The white arrows, white open arrows, and yellow arrows in the "2 min" image panels mark GFP$^+$ mCherry$^-$, GFP$^-$ mCherry$^+$, and GFP$^+$ mCherry$^+$ puncta on the surface of the phagosome, respectively.
(B) DIC and fluorescence images of an embryo exhibiting LGG$^+$ puncta outside phagosomes in multiple cells. The scale in (a) bar is 10 μm. The white arrows, white open arrows, and yellow arrows mark GFP$^+$ mCherry$^-$, GFP$^-$ mCherry$^+$, and GFP$^+$ mCherry$^+$ puncta on the surface of the phagosome, respectively.

The small GTPase RAB-7 and the HOPS complex are essential for the fusion between autophagosomes and phagosomes

The small GTPase RAB-7 is recruited to the phagosomal membrane shortly after the formation of a *C. elegans* phagosome [19]. RAB-7 is enriched on the surfaces of both phagosomes and lysosomes [19]. Mammalian Rab7 and *C. elegans* RAB-7 mediate the fusion between the maturing phagosome and lysosomes and does that through its effector, the HOPS complex [3,25,39]. In addition, mammalian Rab7 is known to drives lysosome-autophagosome fusion through the HOPs complex and PLEKHM1, an adaptor protein [40,41]. *C. elegans* RAB-7 also plays an essential role in autolysosome formation [26], although whether it is localized to autophagosomes was not reported previously. To examine whether RAB-7 is localized to LGG-1$^+$ and LGG-2$^+$ autophagosomes that fuse to *C. elegans* phagosomes, we generated two transgenic *C. elegans* strains that co-expressed the mCherry::LGG-1/ GFP::RAB-7 or mCherry::LGG-2/ GFP::RAB-7 pairs of reporters (**Materials and Methods**). We observed that GFP::RAB-7 was localized to some but not all of the LGG-1$^+$ or LGG-2$^+$ puncta (**Fig 7 B-D**). The LGG$^+$ RAB-7$^+$ double-positive autophagosomes were observed both freely distributed in the cytoplasm of ventral hypodermal cells (**Fig 7B(a-c)** and **C**) and on phagosomal surfaces (**Fig 7B(d-f)** and **D**). In addition, **Fig 7B(d-f)** depicts that GFP::RAB-7 is both evenly distributed to the surface of a phagosome

(d) as previously reported [19], and highly enriched on a LGG-1$^+$ autophagosomes that are recruited to the phagosomal surface (d-f, white arrows). **Fig 7D** shows a dynamic fusion event of an LGG-2$^+$/RAB-7$^+$ punctum (marked by the bottom arrow in the "0 min" time point) attached to the phagosome membrane and becoming part of the phagosomal surface at the "+6 min" time point. On the other hand, we also observed puncta that were LGG$^+$ but RAB-7$^-$ (Fig 7 B and C, white arrowheads), which were likely autophagosomes not acquired RAB-7 yet, and puncta that were LGG$^-$ but RAB-7$^+$ (Fig 7 B and C, yellow arrows), which represented intracellular organelles such as late endosomes or lysosomes. In conclusion, RAB-7 is localized to the majority but not all autophagosomes; furthermore, all autophagosomes that were observed on phagosomal surfaces were RAB-7$^+$.

We next examined whether the recruitment and fusion of LGG-1$^+$- or LGG-2$^+$- autophagosomes to the C1, C2, and C3 phagosomes were normal in *rab-7(ok511)* null mutant embryos [19]. The recruitment event was measured by The enrichment of mCherry$^+$ puncta on the surfaces of phagosomes indicates the recruitment event, whereas the accumulation of the mCherry signal inside the phagosomal lumen indicates the fusion event. In *rab-7(ok511)* mutants, robust enrichment of both the mCherry::LGG-1$^+$ and ::LGG-2$^+$ puncta to phagosomal surfaces are prominent (**Fig 7 E-F**), indicating that the recruitment of autophagosomes was normal. However, no mCherry signal was observed entering the phagosomal lumen (**Fig 7 E-F, Movies S4, S5**). We quantified the time between the moment a phagosome was sealed to that when an unmistakable mCherry signal was observed in the phagosomal lumen by eye. In the wild-type embryos, this time is <30 min in 100% of the samples analyzed, and the median value is 14 and 18 min for LGG-1$^+$ and LGG-2$^+$ autophagosomes, respectively (**Figs 1**(**E** and **H**) and **7(G-H)**). In stark contrast, in *rab-7* mutants, the mCherry signal was not detected in the lumen of any of the phagosomes for LGG-1 or LGG-2 reporters (n=9 for each reporter) over a time span of 0-60 min after phagosome formation (**Fig 7 G-H**). For over half of the samples, the observation period was extended beyond 90 min after phagosome formation, and still, no mCherry signal was observed in the phagosomal lumen within the entire observation period. These results strongly indicate that RAB-7 function is absolutely needed for autophagosomes/phagosome fusion but not required to recruit autophagosomes.

In *C. elegans*, a null mutation in *vps-18*, which encodes VPS-18, a subunit of the HOPs complex, impairs phagosome maturation [42]. The autophagosome-phagosome fusion block observed in *rab-7* mutants rendered us to subsequently examine the *vps-18* null mutant embryos. We found that, like in *rab-7* mutants, the recruitment of autophagosomes to phagosomes appeared normal in *vps-18* mutants (**Fig 7 E-F**). Also, like in *rab-7* mutants, in *vps-18* mutants, the fusion of LGG-1$^+$ and LGG-2$^+$ autophagosomes to phagosomes was severely defective (**Fig 7 E-H**). However, whereas in *rab-7* mutants, the entry of mCherry signal to phagosomal lumen was blocked completely in all samples, in some *vps-18* mutant embryos, the entry of mCherry signal still occurred, *albeit* severely delayed. In contrast, in other samples, the entry was blocked **(Fig 7 E-H)**, indicating a fusion defect that is less severe than that displayed in *rab-7* mutants and suggesting the existence of the residue HOPs function in *vps-18* mutants. Together, our above observations indicate that RAB-7 and the HOPs complex, its effector, play a critical and specific role in the fusion between autophagosomes and phagosomes.

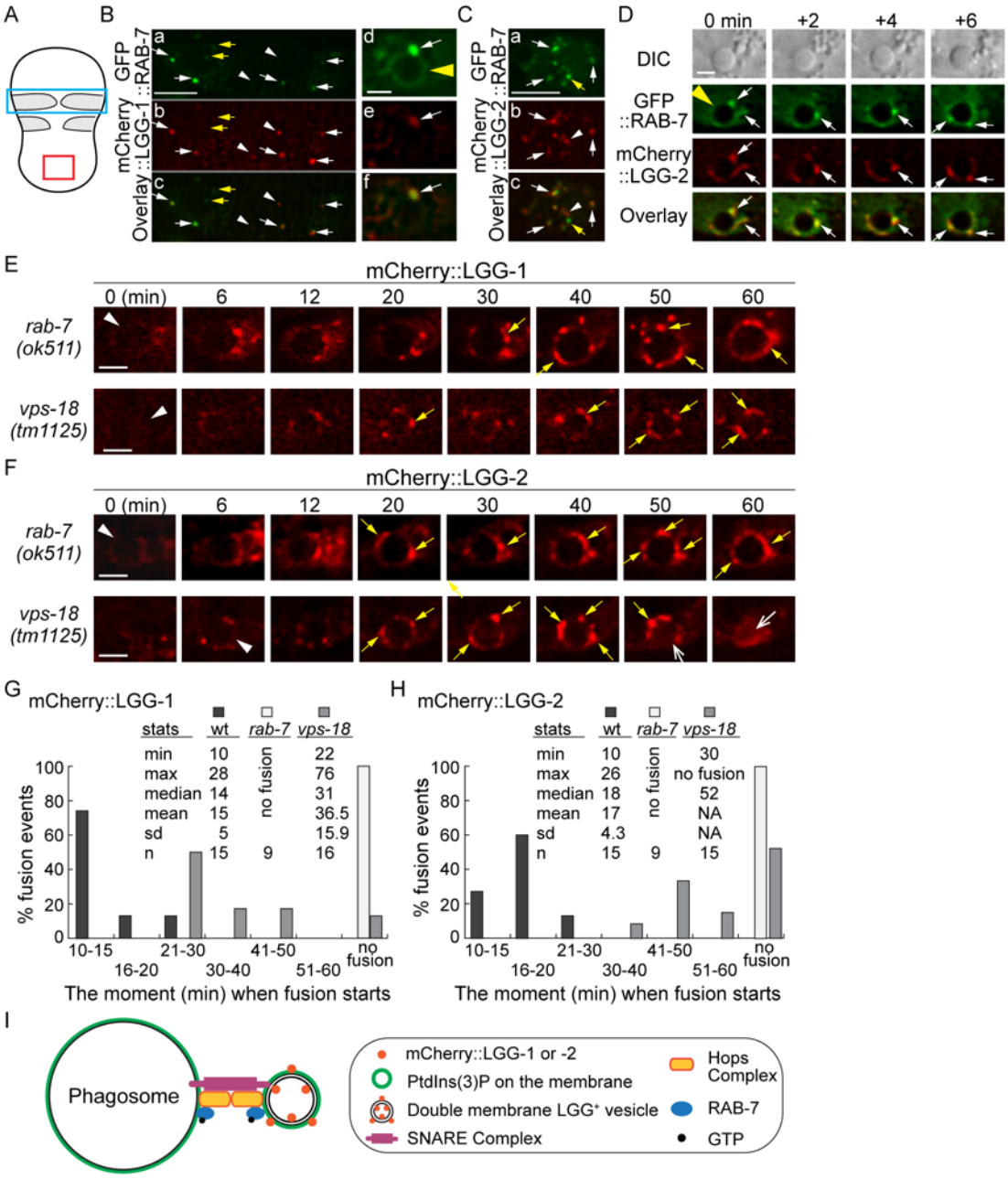

Figure 7. RAB-7 and VPS-18 are essential for the fusion between autophagosomes and phagosomes.
(A) Diagram of the ventral surface of an embryo at ~330 min post 1st embryonic division.
(B-D) Images of part of the ventral surface of an embryo co-expressing $P_{ced\text{-}1}$*gfp::rab-7* and $P_{ced\text{-}1}$*mCherry::lgg-1* (B) or $P_{ced\text{-}1}$*mCherry::lgg-2* (C-D). B(a-c) depicts the region framed by the blue box in (A). B(d-f) depicts a C1 phagosome (a yellow arrowhead). C(a-c) depicts the region framed by the red box in (A). (D) A time-lapse image series of a C1 phagosome (a yellow arrowhead) indicates the dynamic recruitment and fusion of GFP and mCherry double-positive puncta to the phagosomal membrane. "0 min" is the moment when the first puncta are observed on the phagosomal surface. White arrows mark several puncta that are both GFP^+ and $mCherry^+$. Yellow arrows mark puncta that are GFP^+ but $mCherry^-$. White arrowheads mark puncta that are GFP^- but $mCherry^+$. Scale bars for B(a-c) and (C) are 5 μm, and for B(d-f) and (D) are 2 μm.

(E-F) Time-lapse images monitoring the recruitment and fusion of puncta labeled with mCherry::LGG-1 (E) or::LGG-2 (F) to the C1, C2, and C3 phagosomes in *rab-7(ok511)* and *vps-18(tm1125)* mutant embryos. "0 min" represents the moment when a phagosome just seals (white arrowheads). Yellow arrows mark the mCherry$^+$ puncta on the phagosomal surfaces. One open white arrow marks the mCherry signal inside the phagosomal lumen. Scale bars are 2 μm.
(G-H) Histograms depicting the distribution of the time it takes for LGG-1$^+$ or LGG-2$^+$ puncta to fuse to phagosomes, measured from the "0 min" point to the time point when mCherry was detected in the center of a phagosome. C1, C2, and C3 phagosomes were recorded. *n*, the number of phagosomes scored. "No fusion": no mCherry signal entry was observed even after 72-114 min post-nascent phagosome formation. NA: not applicable.
(I) A Diagram depicting the mechanism driving autophagosome-phagosome fusion. RAB-7 is enriched on the surfaces of both phagosomes and autophagosomes. RAB-7 and VPS-18, a subunit of the HOPs complex, are proven essential for autophagosome-phagosome fusion. Other factors are proposed to play roles in this event based on the knowledge of intracellular membrane fusion in general.

The CED-1 pathway drives the recruitment of autophagosomes to phagosomes

The signaling pathway led by the phagocytic receptor CED-1 plays essential roles in initiating the maturation of phagosomes containing apoptotic cells [19]. Two of the events driven by the CED-1 pathway are the incorporations of early endosomes and lysosomes to phagosomes [19,21]. Here we further examined whether the loss-of-function mutations in members of the CED-1 pathway affect the incorporation of autophagosomes to phagosomes. In *ced-1(e1735)* null mutant embryos [20] that express the mNG::LGG-1 or -2 reporters, we observed severe defects in the incorporation of autophagosomes into phagosomes. First of all, only a very dim mNG signal was observed inside the phagosomal lumen 50 min post phagosome formation, a time point well past the observed initiation time for autophagosomes/phagosome fusion in wild-type condition (**Fig 8 A**, **C**, **F**, and **G, Movie S6**). Whereas in wild-type embryos, the median relative LGG-1 and -2 signal intensities are 6.3 and 5.3 at 50 min-post phagosome formation, respectively, in *ced-1* mutant embryos, the median values are merely 2.1 and 1.6, respectively (**Fig 8 K-L**). Secondly, unlike in *rab-7* mutants, where autophagosomes were observed accumulating on phagosomal surfaces (**Fig 7**), in *ced-1* mutants, very few LGG-1- or LGG-2-labeled puncta were observed on phagosomal surfaces (**Fig 8 A**, **C**).

Further quantitative measurement of the samples presented in (**Fig 8 A**, **C**) and 14 additional samples for each of the reporters confirmed that the mNG signal was not enriched on the surfaces of phagosomes, in contrast to wild-type embryos (**Fig 8 I-L**). These results indicate a severe defect in the recruitment of autophagosomes to phagosomes. Unlike in the *atg* mutants that we have examined (**Figs S1** and **S2**), in *ced-1* mutant embryos, normal numbers of LGG-1$^+$ or LGG-2$^+$ puncta were observed (**Fig S6**), indicating normal biogenesis of autophagosomes. Thus the recruitment defect observed in *ced-1* mutants is not a consequence of the lack of autophagosomes; instead, it is likely a result of a certain defect in signaling between phagosomes and autophagosomes.

We further examined whether CED-6 and DYN-1, two other members of the CED-1 pathway, were also needed for the incorporation of autophagosomes into phagosomes. In the *ced-6(n2095)* and *dyn-1(n4039)* mutant embryos, the median relative LGG-1 and LGG-2 signal intensities in the center of phagosomes are much lower than that in wild-type samples, respectively, at 50 min-post phagosome formation mutants (**Figs 8(B, D, F, G, K-L)** and **9(A, D E, F, I, J)**), although the defects are not as severe as in *ced-1* mutants (**Fig 8(A,**

C, F, G, K, L)). Further observation discovered that the LGG-1 or LGG-2-labeled puncta were rarely observed on the surfaces of phagosomes in these mutants (**Figs 8(B, D, I, J)** and **9(A, F)**), demonstrating severe defects in the recruitment of autophagosomes to phagosomal surfaces.

In *ced-1*, *ced-6*, and *dyn-1* mutants, the fusion between autophagosomes and phagosomes might also be defective. However, the severe recruitment defects resulted in the lack of LGG-labeled puncta on phagosomal surfaces, making it difficult to evaluate whether there were additional fusion defects and how severe the fusion defects were.

We also examined whether the pathway composed of the small GTPase CED-10 and its bipartite Guanine Nucleotide Exchange Factor (GEF) CED-5 and CED-12, which acts parallel to the CED-1 pathway in the engulfment of cell corpses, plays any role in promoting the incorporation of autophagosomes into phagosomes. In the *ced-5(n1812)* null mutant and *ced-10(n1993)* loss-of-function mutant embryos, the accumulation of the LGG-1 and LGG-2 signals on the surfaces of the phagosomes and the subsequent accumulation of signals inside phagosomal lumen were normal both in the time course and in the levels of signal enrichment (**Fig 9 B, C-E, G, H-J**), indicating that both the recruitment of autophagosomes to phagosomal surfaces and the subsequent fusion between autophagosomes and phagosomes are normal. We thus conclude that, unlike the CED-1/-6/DYN-1 pathway, the CED-5/-10 pathway is not involved in regulating the incorporation of autophagosomes to phagosomes (**Fig 9K**).

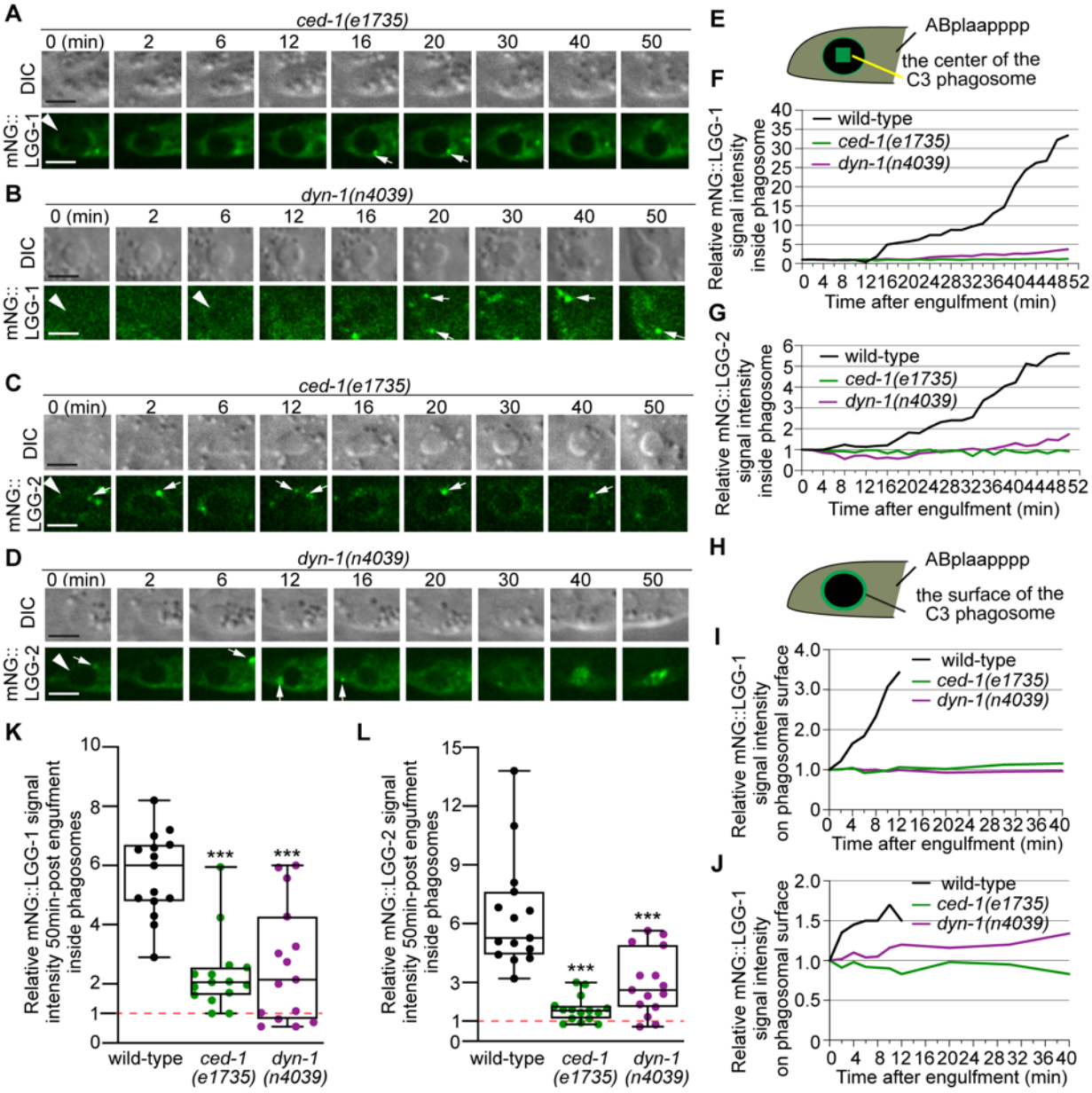

Figure 8. CED-1 and DYN-1 are essential for the incorporation of autophagosomes into phagosomes
(A-D) Time-lapse image series monitoring the presence or absence of puncta (white arrows) labeled with mNG::LGG-1 (A-B) or -2 (C-D) on C3 phagosomes (white arrowheads) and the subsequent entry of the mNG signal into the lumen in *ced-1* and *dyn-1* mutant embryos. DIC images mark the position of the cell corpse. "0 min" is the moment when phagosomes are just sealed. Scale bars are 2μm.
(E) A diagram illustrating that the relative mNG signal in the center of a phagosome is measured over time to create sub-figures (F) and (G). At time point t (time after "0 min"), the Relative Signal Intensity $_T$ = (Unit Intensity(phagosome center)$_T$ –Unit Intensity(background)$_T$) / (Unit Intensity(phagosome center)$_{T0}$- Unit Intensity (background)$_{T0}$).
(F-G) The relative mNG::LGG-1 (F) or -2 (G) signal intensity in the center of a phagosome (Y-axis) over time in the 2-min interval (X-axis). "0 min" is the moment when pseudopods are sealed and a nascent phagosome forms. (F) The data for the wild-type, *ced-1(e1735),* and *dyn-1(n4039)* mutant embryos are from Figs 1F and

8(A-B), respectively. (G) The data for the wild-type, *ced-1(e1735),* and *dyn-1(n4039)* mutant embryos are from Figures 1I and 8(C-D), respectively.

(H) A diagram illustrating that the relative mNG signal on the surface of a phagosome is measured over time to create sub-figures (I) and (J). At time point T (time after "0" min), the Relative signal intensity $_T$ = (Unit Intensity(phagosome surface (the green ring))$_T$ –Unit Intensity(background)$_T$) / (Unit Intensity(phagosome surface)$_{T0}$ - Unit Intensity (background)$_{T0}$).

(I-J) The relative mNG::LGG-1 or -2 signal intensity on the surface of a phagosome (Y-axis) over time in the 2-min interval (X-axis). "0 min" indicates the moment when pseudopods are sealed and nascent phagosome forms. (I) The data for the wild-type, *ced-1(e1735),* and *dyn-1(n4039)* mutant embryos are from Figures 1F and 8(A-B), respectively. (J) The data for the wild-type, *ced-1(e1735),* and *dyn-1(n4039)* mutant embryos are from Figs 1I and 8(C-D), respectively.

(K-L) Box-and-Whiskers plots of the relative mNG signal intensity measured in the center of phagosomes 50 min-post the formation of nascent C3 phagosomes from 15 each of wild-type, *ced-1(e1735),* and *dyn-1(n4039)* mutant embryos. Red dashed lines indicate the position of value 1, which represents no signal enrichment relative to the background signal. ***, $p<0.001$, Student *t*-test of each mutant compared to the wild-type value.

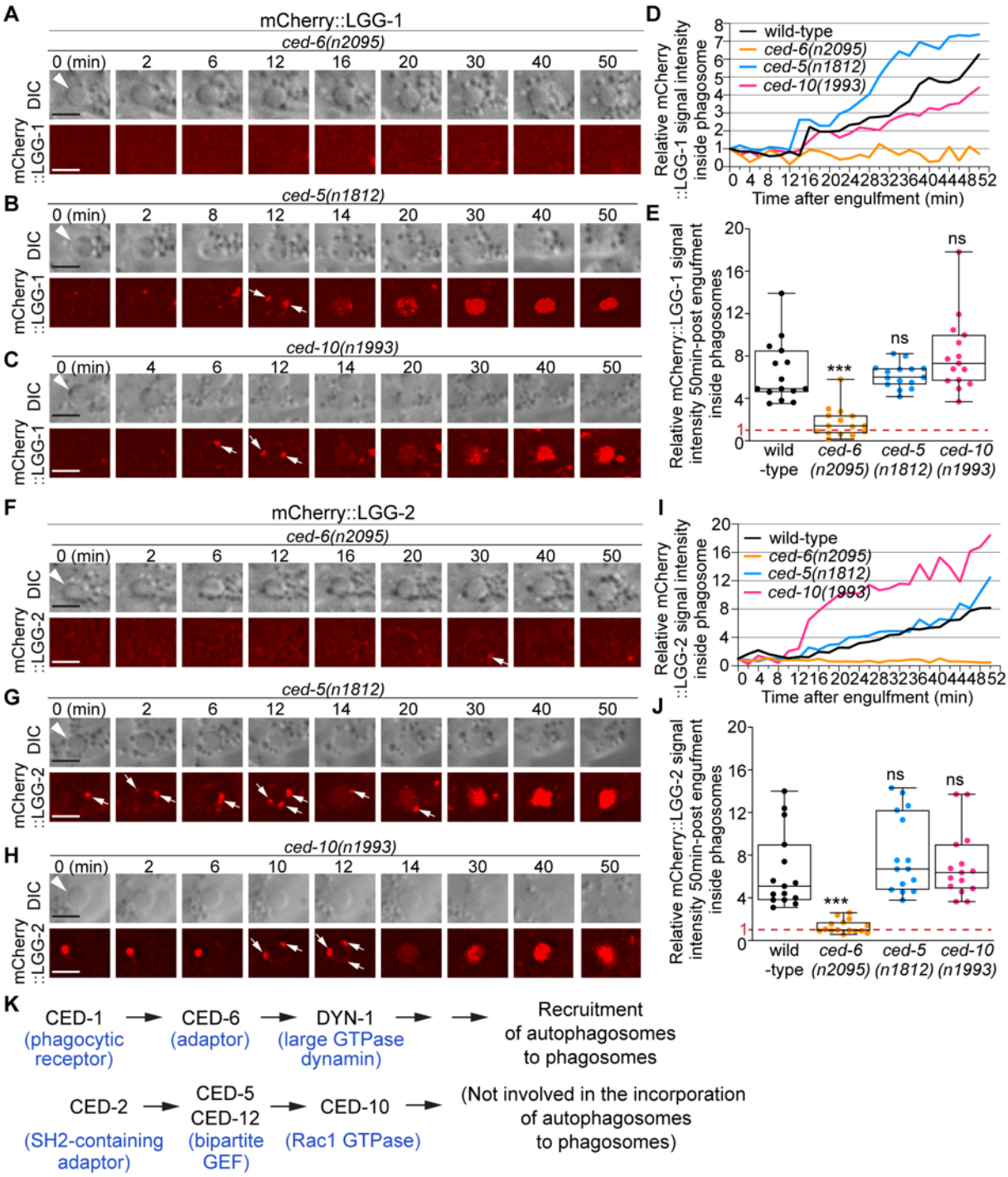

Figure 9. *ced-6*, but not *ced-5* or *ced-10*, is required for the incorporation of autophagosomes into phagosomes

(A-C and F-H) Time-lapse image series monitoring the presence or absence of puncta (white arrows) labeled with mCherry::LGG-1 (A-C) or -2 (F-H) on C3 phagosomes (white arrowheads) and the subsequent entry of the mCherry signal into the phagosomal lumen in *ced-6*, *ced-5*, and *ced-10* mutant embryos. DIC images mark the position of the cell corpse. "0 min" is the moment when a nascent phagosome just seals. Scale bars are 2μm.

(D and I) The relative mCherry::LGG-1 (D) or -2 (I) signal intensity in the center of a phagosome (Y-axis) over time (in the 2-min interval) (X-axis). "0 min" indicates the moment when a nascent phagosome just seals. (D) The data for the wild-type, *ced-6(n2095), ced-5(n1812),* and *ced-10(n1993)* mutant embryos are from Figs 1E and 9(A-C), respectively. (I) The data for the wild-type, *ced-6(n2095), ced-5(n1812),* and *ced-10(n1993)* mutant embryos are from Figs 1H and 9(F-H), respectively.
(E and J) Box-and-Whiskers plots of the relative mCherry signal intensity measured in the center of phagosomes 50 min-post the formation of nascent C3 phagosomes from 15 each of wild-type, *ced-6(n2095), ced-5(n1812),* and *ced-10(n1993)* mutant embryos. The Red dashed lines indicate where value 1, which represents no signal enrichment relative to the background signal, stand. "***", $p<0.001$; ns, not significant, Student *t*-test against the wild-type samples.
(K) A diagram illustrating that between the two parallel pathways that regulate the clearance of apoptotic cells, only the CED-1 pathway, but not the other pathway, plays an essential role in promoting the incorporation of autophagosomes into phagosomes. Blue letters in parentheses are the names of the mammalian homolog of the corresponding *C. elegans* proteins.

The incorporation of lysosomes into phagosomes is not affected by the lack of autophagosomes
The incorporation of lysosomes is an essential force that drives the degradation of phagosomal contents [3]. Because a portion of the autophagosomes would fuse with lysosomes and become autolysosomes that retain lysosomal features [9], it is possible that the LGG^+ particles, which include both autophagosomes and autolysosomes, might act to provide additional vesicles bearing lysosomal features (such as autolysosomes) to fuse to phagosomes. We thus examined whether mutations that specifically impair autophagosomes biogenesis would affect the amount and timing of organelles with lysosomal features, including lysosomes and autolysosomes, that are incorporated into phagosomes. *C. elegans* NUC-1 is an endonuclease belonging to the DNase II family and resides in the lysosomal lumen [43,44]. We used a *nuc-1::mCherry* reporter expressed in engulfing cells under the control of P_{ced-1} to quantify the rate of lysosome-phagosome fusion. In time-lapse recording images monitoring phagosomes containing cell corpses C1, C2, and C3 in wild-type embryos expressing NUC-1::mCherry, we observed the attachment of mCherry puncta on the surfaces of phagosomes and the subsequent accumulation of the mCherry signal into the phagosomal lumen (Fig 10A). This dynamic process represents the recruitment and the subsequent fusion of lysosomal particles to phagosomes and the delivery of NUC-1::mCherry into the phagosomal lumen. To compare with wild-type samples, we measured the signal level of NUC-1::mCherry in the center of phagosomes in *lgg-1(tm3489)*, *lgg-2(tm5755)*, and *atg-7(bp411)* embryos over time and observed accumulation of mCherry signal in the phagosomal lumen in all samples (**Fig 10 A-E**). These three mutants are defective in the biogenesis of autophagosomes. Quantitative analysis of 15 phagosomes of each genotype found that, 60 min after the formation of the nascent phagosomes, (1) no significant difference in the mCherry signal level in the phagosomal lumen in *lgg-2* mutants compared to wild-type samples (**Fig 10F**), and (2) slight elevation of the mCherry signal in the lumen of *lgg-1* and *atg-7* mutant samples. In addition, the median value of the first time point when NUC-1::mCherry signal was detected inside the phagosomal lumen was not significantly different in all four genotypes (**Fig 10G**). All these data demonstrate that the incorporation of lysosomes into phagosomes is normal in *lgg-1*, *lgg-2*, and *atg-7* mutants. Therefore, defects in the formation of autophagosomes, which would result in the lack of autolysosomes, do not affect the incorporation of lysosomes into phagosomes.

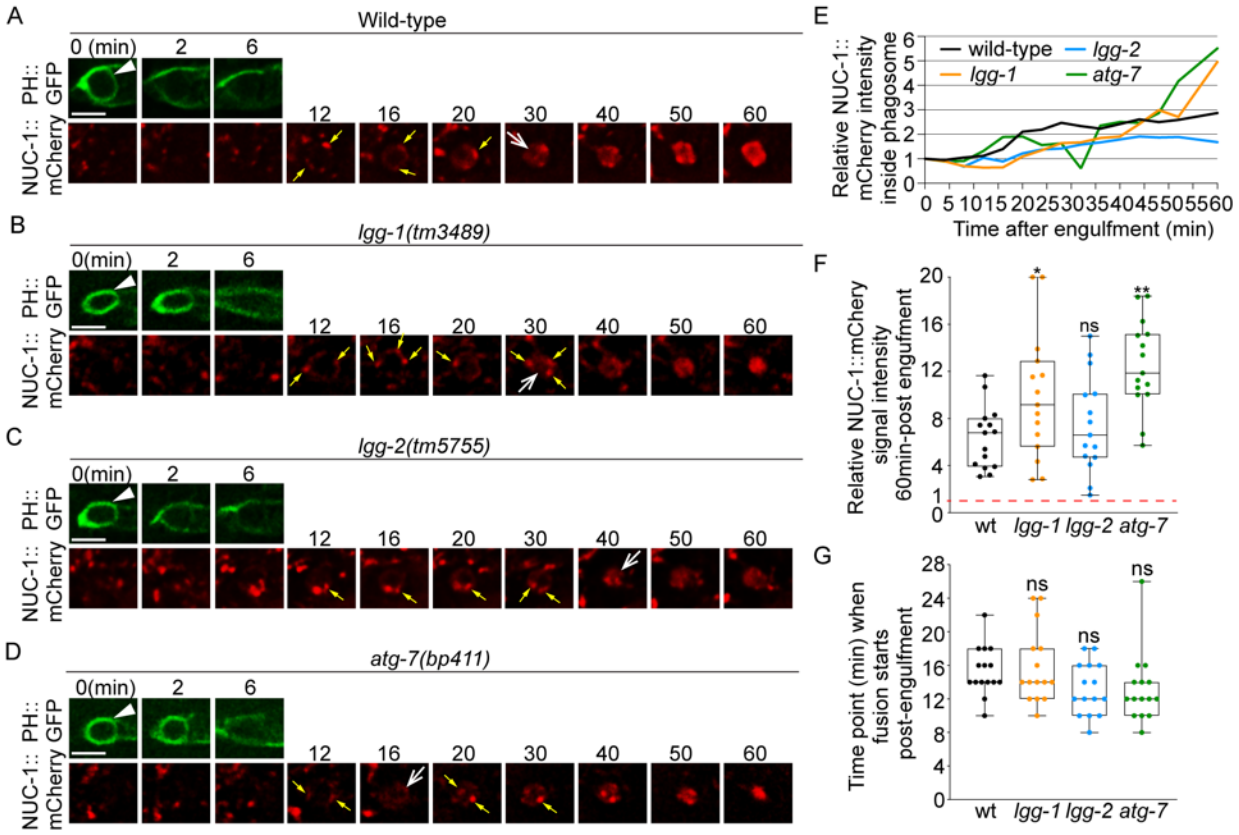

Figure 10. Defects in the formation of autophagosomes do not affect the timing or efficiency of lysosomes incorporation into phagosomes

The time-lapse recording was conducted on phagosomes containing C1, C2, and C3 in wild-type and named mutant embryos carrying $P_{ced\text{-}1}$*nuc-1::mCherry*, the lysosomal lumen reporter, and $P_{ced\text{-}1}$*PH(PLCγ)::gfp*, the marker for extending pseudopods and nascent phagosomes. (A-D) Fluorescence time-lapse images of one C3 phagosome in each strain with the indicated genotype. "0 min" is the moment when a nascent phagosome (white arrowhead) just seals. Yellow arrows mark the lysosomal particles that are located on phagosomal surfaces. White open arrows mark the phagosomes with mCherry signals in the lumen. Scale bars are 2.5 μm.

(E) The relative NUC-1::mCherry signal intensity in the center of a phagosome (Y-axis) over time (in 2-min interval) (X-axis). "0 min" indicates the moment when a nascent phagosome is just sealed. Data are from Fig 10 (A-D).

(F) A Box-and-Whiskers graph of the relative mCherry signal intensity measured in the center of phagosomal lumen 60 min-post the formation of nascent C3 phagosomes from 15 each of wild-type, *lgg-1(tm3489), lgg-2(tm5755),* and *atg-7(bp411)* mutant embryos. A dashed red line marks the position where the relative signal intensity value =1, which indicates no enrichment of mCherry signal inside the phagosomal lumen.

(G) A Box-and-Whiskers graph displaying the first time point when the NUC-1::mCherry signal is detected inside the lumen of 15 C3 phagosomes in wild-type, *lgg-1(tm3489), lgg-2(tm5755),* and *atg-7(bp411)* mutant embryos.

Discussion

We have identified autophagosomes as a new kind of intracellular organelles that contribute to the degradation of phagosomal contents. In *C. elegans* hypodermal cells that engulfed apoptotic cells, autophagosomes are recruited to the surfaces of phagosomes and subsequently fuse to the phagosomal membrane. Through this previously unknown interaction, autophagosomes release substances to the phagosomal lumen and membrane. We have further identified a signaling pathway that promotes the recruitment and subsequent fusion of autophagosomes to phagosomes. Together, these findings reveal a novel mechanism through which the pathways that control autophagy and phagocytosis converge, underlining the importance of this mechanism in the degradation of apoptotic cells.

Canonical autophagosomes play an essential role in the degradation of apoptotic cells

Previously, *C. elegans* autophagy genes have been implicated in facilitating the clearance of apoptotic cells. Autophagy occurring in apoptotic cells was implicated in facilitating the exposure of phosphatidylserine, the "eat me" signal that attracts engulfing cells, to the surfaces of apoptotic cells in mice embryonic bodies and *C. elegans* [45,46]. Multiple autophagy genes were reported to participate in the clearance of apoptotic cells in *C. elegans* engulfing cells [11-13,46]. They were reported to work together with Class II PtdIns3 kinase PIKI-1 [11], to facilitate the recruitment of two small GTPases RAB-5 and RAB-7 to phagosomal surfaces [13, and to promote phagosome degradation [46]. The above findings suggest that the corresponding autophagy genes might have separate functions in the degradation of phagosomal contents in addition to their canonical roles in autophagosome biogenesis. Our work reported here presents a different discovery regarding how the autophagy machinery regulates phagosome degradation.

We found that the canonical double-membrane autophagosomes actively participate in the degradation of apoptotic cells inside phagosomes. Four critical sets of evidence indicate that the LGG-1- and -2-labeled vesicles that are incorporated into phagosomes are autophagosomes, not LAP vesicles. First, the membrane-bound LGG-1 or -2 reporters were observed to enter the phagosomal lumen after vesicle-phagosome fusion. Only when the vesicles are of double membranes and when the reporter molecules label both the inside and outside membranes, the entry of the signal into phagosomal lumen is possible (**Fig 1K**). Conversely, if the LGG-1 or -2 labeled vesicles are of a single membrane, after vesicle-phagosome fusion, the reporter signal would remain on the phagosomal membrane, as the membrane-bound lysosomal marker CTNS-1::mRFP does (**Fig 1K**). Secondly, these vesicles are also labeled with GFP-tagged ATG-9, an integral membrane protein inserted in autophagosomal membranes. Thirdly, the production of these vesicles relies on genes pivotal for autophagosome biogenesis, such as *atg-3*, *atg-7*, and *atg-9*. Last but not least, genes encoding the *C. elegans* homologs of mammalian ULK1, ATG13, and ATG14, which are dispensable for the generation of LAP vesicles in mammalian cells [6], are required for the efficient clearance of apoptotic cells and for the formation of the LGG-labeled vesicles discussed here, further verifying that these vesicles are distinct fro the single-membrane LAP vesicles. Together, these findings verify that double-membrane autophagosomes, not single-membrane LAP vesicles, are being incorporated into phagosomes.

In *C. elegans*, LC3-dependent phagocytosis was reported to function in the clearance of the midbody, a structure that is essential for the completion of cytokinesis, and the second polar body generated during female meiosis [47,48]. The clearance of midbodies and second polar body is considered independent of autophagy based on the observation that neither *unc-51* nor *epg-8* is required for the above processes [47,48]. However,

since whether the LGG markers attached to phagosomes carrying midbodies or polar bodies are attached to double-membrane or single-membrane vesicles has not been investigated [47,48], whether LAP vesicles exist in C. elegans cells still needs to be demonstrated.

In mammalian cells, besides LAP vesicles, perhaps canonical autophagosomes also contribute to the degradation of apoptotic cells in phagosomes. The demonstration of an autophagosome-phagosome fusion event in *C. elegans*, a well-established model organism for the study of cell death-related events, opens a path to investigate whether autophagosome-phagosome fusion is an evolutionarily conserved event. In addition, the autophagosome-phagosome fusion might contribute to the degradation of other kinds of phagosomal cargos besides apoptotic cells.

The observation of the LGG-1 or -2 signals inside the phagosomal lumen owes to the choice of mCherry as a reporter tagged to LGG-1 and -2. The mCherry protein is resistant to acidic pH [30]. Phagosome luminal pH value reduces from 5.5-6.0 to 4.5-5.5 after incorporating lysosomes [49], leading to the inactivation of the fluorophore of the commonly used GFP reporter [29]. In fact, in *C. elegans* engulfing cells, GFP-tagged LGG-1 or -2 are only observed on the surfaces but not in the lumen of phagosomes, presumably due to the acidic environment of the phagosomal lumen (**Fig 1**). It is thus conceivable that in other experimental systems, a mCherry-tagged LC3 marker might disclose a previously overlooked fusion between autophagosomes and phagosomes.

LGG-1 and LGG-2 define three subpopulations of autophagosomes that are incorporated into phagosomes

LGG-1 and -2 are close homologs, and each labels autophagosomes. We have observed three separate classes of autophagosomes that are incorporated into phagosomes: LGG-1$^+$ LGG-2$^-$, LGG-1$^-$ LGG-2$^+$, or LGG-1$^+$ LGG-2$^+$. These subpopulations might represent autophagosomes at different stages of maturation [26]. Remarkably, we have found that the *lgg-1*; *lgg-2* double mutants display a much enhanced Ced phenotype than that displayed by each of the *lgg-1* or *lgg-2* single mutants. Together, these results indicate that autophagosomes at different stages of maturity all contribute to the degradation of apoptotic cells.

What do autophagosomes contribute to the degradation of apoptotic cells

We have found that blocking the biogenesis of autophagosomes or the recruitment of autophagosomes to phagosomes results in a significant delay in the degradation of phagosomal content and, consequently, the persistent appearance of engulfed cell corpses. The incorporation of autophagosomes into phagosomes presumably delivers certain substances to the lumen and/or membrane of phagosomes, substances that are important for the degradation of phagosomal contents. Currently, the identities of these substances are still a mystery. Studies in mammalian cells implicate LAP vesicles in facilitating the incorporation of lysosomes into phagosomes [5,6]. In *C. elegans* mutants defective for the biogenesis of autophagosomes (*atg-7*, *lgg-1*, and *lgg-2* mutants), we found no decrease in the accumulation of the lysosomal lumen protein NUC-1::mCherry in the phagosomal lumen in terms of the total amount and rate of accumulation (**Fig 10**), indicating that lack of autophagosomes does not affect the efficiency of lysosome-phagosome fusion. This result, together with the observation that the three subpopulations of autophagosomes at different maturation stages all fuse to phagosomes, suggests that it is not just the sub-population of autolysosomes, which have lysosomal features, that contribute to phagosomal degradation. Thus autophagosomes might deliver something unique to the phagosome, something not present in lysosomes or endosomes. These substances also might not be limited to

proteins in the autophagosome lumen or membranes; they could be specific lipid molecules from the membranes of autophagosomes. Further investigation is required to discover the identities of this (these) molecule(s).

The CED-1 signaling pathway drives the incorporation of autophagosomes to phagosomes

Autophagosomes are incorporated into phagosomes in two sequential steps: (1) the recruitment to the phagosomal surfaces, which can be detected by the enrichment of punctated LGG-1 or -2 fluorescence reporters on phagosomal surfaces, and (2), the subsequent fusion, which is detected by the enrichment of the LGG-1 or -2 reporter signals inside the phagosomal lumen. RAB-7 and its effector, the HOPS complex, are known to act as tethering factors that facilitate the fusion of various intracellular organelles, including autophagosomes, to lysosomes [26,50]. Relevant to this study, RAB-7 and VPS-18 are pivotal for the fusion between lysosomes and phagosomes and for the degradation of apoptotic cells inside phagosomes in *C. elegans* [19,42,51]. We have discovered that RAB-7 and VPS-18 play essential and specific roles in the fusion but not for the recruitment of autophagosomes to phagosomes. Our finding adds a new pair of organelles that depend on the RAB-7/HOPS complex for fusion to each other. As RAB-7 is enriched on the surfaces of both phagosomes and autophagosomes ([19] and (**Fig 7(B-D)**), and as the HOPS complexes in mammalian cells and Drosophila are known to interact with the SNARE complex, the membrane fusion machinery [52,53], we propose that the RAB-7/HOPS complex acts on the surfaces of phagosomes and autophagosomes to facilitate autophagosomes-phagosome fusion via promoting the interaction between the SNARE complexes on phagosomes and autophagosomes (**Fig 7I**).

The CED-1 signaling pathway, which initiates the maturation of phagosomes that bear apoptotic cells, is essential for the enrichment of GTP-bound RAB-7 to the surfaces of phagosomes [19]. Here we have found that CED-1, CED-6, and DYN-1 drive the incorporation of autophagosomes to phagosomes, in addition to the incorporation of early endosomes and lysosomes previously discovered [19,21]. In *ced-1* mutants, for example, the recruitment of autophagosomes to the surfaces of phagosomes is almost completely blocked. Due to the severe recruitment defect, whether the *ced-1* null mutation further impairs the fusion between autophagosomes and phagosomes cannot be readily visualized. However, since a *ced-1* null mutation impairs the recruitment of RAB-7 to [19] and the production of PtdIns(3)P on phagosomal surfaces [19,23], and since the recruitment of the HOPS complex to the surfaces of intracellular organelles requires both RAB7 and PtdIns(3)P [39,54,55], we predict that the CED-1 pathway would control the RAB-7/HOPS complex-mediated autophagosomes-phagosome fusion. Identifying the CED-1 signaling pathway as the driving force for the incorporation of autophagosomes to phagosomes helps to reveal the molecular mechanisms behind the crosstalk between autophagy and phagocytosis.

Materials and Methods

Mutations, strains, and transgenic arrays

C. elegans strains were grown at 20ºC as previously described [56] unless indicated otherwise. The N2 Bristol strain was used as the wild-type control strain. Mutations are described in [57] and by the Wormbase (http://www.wormbase.org) unless noted otherwise (**Table S1**): LG1: *ced-1(e1735), epg-8(bp251)*; LGII: *lgg-1(tm3489), rab-7(ok511), vps-18(tm1126)*; LGIII: *atg-13(bp414), ced-6(n2095);* LGIV: *atg-3(bp412), atg-7(bp411), ced-5(n1812), ced-10(n1993), lgg-2(tm5755* and *tm6474)*; LGV: *atg-9(bp564), atg-18(gk378), unc-*

76(e911), unc-51(e369); LGX: *atg-2(bp576), dyn-1(n4039). dyn-1(n4039)* homozygous mutants, which are zygotic embryonic lethal, were maintained by an extrachromosomal array carrying a wild-type *dyn-1* gene and a co-expressed P_{egl-13}*gfp* marker (**Table S1**) [21]. *dyn-1(n4039)* homozygous embryos losing the rescuing transgene were identified as the embryos not carrying P_{egl-13}*gfp*. The *rab-7(ok511) and lgg-1(tm3489)* homozygous strains are both maternal-effect embryonic lethal, and the mIn1 balancer maintained each allele with an integrated pharyngeal GFP marker (**Table S1**) [58]. To obtain *rab-7(ok511)* m^-z^- homozygous embryos, GFP^- *rab-7(ok511)* homozygous hermaphrodites were isolated among the progeny of the strain VC308, and their progeny were collected as embryos. The same protocol was used to collect *lgg-1(tm3489)* m^-z^- embryos from the strain GK738 (**Table S1**). Double mutants between *lgg-1(tm3489)/mIn1* and *lgg-2(tm6474)* were generated by standard genetic crosses.

Extrachromosomal arrays were generated by the microinjection of plasmids with the co-injection marker p76-18B [*punc-76(+)*] into *unc-76(e911)* mutants [59,60]. Non-Unc mutants were identified as transgenic animals. Integrated transgenic arrays were generated by gamma irradiation [60]. Integrated arrays generated in this study are as follows (**Table S1**): LGI: *enIs87[*P_{ced-1}*PH(hPLCγ)::mrfp* and P_{ced-1}*mNG::lgg-1];* LGII: *enIs82[*P_{ced-1} *ced-1::gfp* and P_{ced-1} *mCherry::lgg-1];* LGV: *enIs85[*P_{ced-1} *PH(hPLCγ)::mrfp* and P_{ced-1} *mNG::lgg-2];* LGX: *enIs83[*P_{ced-1} *ced-1::gfp* and P_{ced-1} *mCherry::lgg-2].*

Plasmid construction

lgg-1 and *lgg-2* cDNAs were PCR amplified from a mixed-stage *C. elegans* cDNA library [61]. To generate the P_{ced-1} *gfp::lgg*-1 and P_{ced-1} *gfp::lgg-2* plasmids, *lgg-1* and *lgg-2* cDNAs were cloned into the XmaI and KpnI sites of plasmid pZZ956 (P_{ced-1} *5'gfp)* [61]. P_{ced-1} *mCherry::lgg-1 or -2* were constructed by replacing the cDNA of *gfp* with that of mCherry [30]. P_{ced-1} *mNG (mNeonGreen)::lgg-1 or -2* were constructed by replacing the cDNA of *gfp* with that of mNeonGreen [62]. To generate P_{ced-1}*gfp::lgg-1(G116A)* and P_{ced-1}*gfp::lgg-2(G130A),* the QuickChange Site-directed Mutagenesis Kit (Stratagene, La Jolla, CA) was used to introducing the above mutations into the constructs. To construct P_{ced-1} *atg-9::mCherry, the atg-9a* open reading frame was PCR-amplified from a *C. elegans* mixed-stage cDNA library and inserted between P_{ced-1} and *gfp* in pZZ829 (P_{ced-1} *3'gfp*) [61]. The *gfp* cDNA was then replaced by the *mCherry* cDNA [30]. All plasmids contain an *unc-54* 3' UTR.

Quantification of the number of cell corpses using Nomarski DIC microscopy

Cell corpses display a highly refractive button-like morphology under Differential Interference Contrast (DIC) microscopy. An Axionplan 2 compound microscope (Carl Zeiss, Thornwood, NY) equipped with Nomarski DIC optics, an AxioCam digital camera, and AxioVision imaging software was used for DIC microscopy. Using a previously established protocol [27], we quantified the number of cell corpses in the head region at the 1.5-fold and 2-fold stage embryos, which are ~420 and ~460 min post-first cleavage.

Fluorescence microscopy and time-lapse imaging

A DeltaVision Elite Deconvolution Imaging System (GE Healthcare, Inc.) equipped with a DIC imaging apparatus and a Photometrics Coolsnap 2 digital camera was used to capture fluorescence, and DIC images Applied Precision SoftWoRx 5.5 software was utilized for deconvolving and analyzing the images [27]. To observe the amount of autophagosomes in ventral hypodermal cells that express P_{ced-1}, fourteen serial Z-

sections in 0.5□1 interval between adjacent optical sections, starting at the ventral surface of embryos at mid-embryonic stages, were collected. The 2D projection image of each Z-stack was generated and compared among different genetic backgrounds (**Figs S1**, **S2**, **S4**, and **S6**). To track fluorescence markers on pseudopods, on the surfaces of phagosomes, or inside phagosomal lumen during the clearance process of cell corpses C1, C2, and C3, embryos were monitored on their ventral surface starting at ~310 min post-first cleavage using an established time-lapse imaging protocol [27]. Twelve to 16 serial *Z*-sections (at 0.5-μm intervals) were captured every 2 min, with recordings typically lasting between 60 to 180 min. Embryos that exhibited normal elongation and movement were considered developing properly. The moment engulfment starts is defined as when the extension of pseudopods around C1, C2, or C3 is first observed. The moment a nascent phagosome form is defined as when the pseudopods around a cell corpse join and make a full closure. The life span of a phagosome is defined as the time interval between the moments when the nascent phagosome forms and when the phagosome shrinks to one-half of its original diameter.

The time spans of the engulfment and degradation processes of cell corpses C1, C2, or C3 were measured as previously established [61]. Briefly, a pseudopod marker, either CED-1::GFP or PH(PLCγ)::GFP, was monitored over time. The moment engulfment starts is defined as when the budding pseudopods around C1, C2, or C3 is first observed. The moment a nascent phagosome form is defined as the moment when the pseudopods around a cell corpse join and make a full closure. The period between the budding and the sealing of the pseudopods is the time span of engulfment. To measure phagosome duration, a co-expressed phagosomal surface marker mCherry::2xFYVE was used to track the diameter of the phagosome over time. The life span of a phagosome is defined as the time interval between the time points when a nascent phagosome was born and when the phagosome shrank to one-half of its original diameter.

Quantitative measurement of signal intensity

Measuring the signal intensity inside the phagosomal lumen

In embryos expressing mCherry- or mNG-tagged LGG-1 or LGG-2, to measure the fluorescence signal intensity inside the phagosomal lumen over time, we identified the boundary of a phagosome and the "0 min" time point when a nascent phagosome was formed by observing the co-expressed marker for a nascent phagosome such as CED-1::GFP or PH(PLCγ)::GFP. At each time point, the total LGG-1 or -2 image intensity of a fixed area (4x4 pixels) at the center of a phagosome ($Int_{phagosome}$) was recorded (**Fig 1C**), so was the intensity of an area of the same size (4x4 pixels) outside the embryo as the background image intensity ($Int_{background}$). The Relative image intensity (RInt) at a particular time point (Tn) comparing to the start point (T0) is calculated as $RInt_{Tn} = (Int_{phagosome}-Int_{background})_{Tn} / (Int_{phagosome}-Int_{background})_{T0}$. The $RInt_{Tn}$ value of 1.0 indicates no entry of LGG-1- or LGG-2-labeled autophagosomes into the phagosomal lumen.

Measuring the signal intensity on the surface of a phagosome

To measure the efficiency of recruitment of autophagosomes to phagosomes, we quantified the intensity of mCherry- or mNG-labeled LGG-1 or LGG-2 on the surfaces of phagosomes. First, we identified the boundary of a phagosome and the "0 min" time point when a nascent phagosome just formed by observing co-expressed CED-1::GFP or PH(PLCγ)::GFP. At a particular time point, Tn or T0, the surface of a phagosome was outlined by two closed polygons (**Fig 8E**). The total signal intensities, as well as the areas of the polygons, were recorded. The unit signal intensity of the "donut-shape" area between the two polygons was calculated as follows:

Unit Intensity ($UI_{phagosome}$) = ($Intensity_{external\ polygon} - Intensity_{internal\ polygon}$)/($Area_{external\ polygon} - Area_{internal\ polygon}$). The Unit Background Intensity ($UI_{background}$) was measured from a polygon outside the embryo was calculated as follow: $UI_{background} = Intensity_{background}/Area_{background}$.
At the time point Tn, the relative signal intensity ($RInt_{Tn}$) = $(UI_{phagosome} - UI_{background})_{Tn}$ / $(UI_{phagosome} - UI_{background})_{T0}$. The $RInt_{Tn}$ value 1.0 indicates no enrichment of LGG-1- or LGG-2-labeled autophagosomes on phagosomal surfaces comparing to the "0 min" time point.

Acknowledgment

We thank Ying Wang for technical support and R. Haley for helpful comments. We thank the *C. elegans* Genetics Center (CGC), funded by the NIH Office of Research Infrastructure Programs (P40 OD010440), for providing some strains. We also thank the National BioResource Project of Japan and Dr. Shohei Mitani for provides some strains.

Funding Source

NIH R01GM067848 supports this work.

Author Contributions

The author(s) have made the following declarations about their contributions: Conceived and designed the experiments: OPR ZZ. Performed the experiments: OPR LC XL HH ZZ. Analyzed the data: OPR ZZ. Prepare the manuscript: OPR ZZ.

Supplemental material

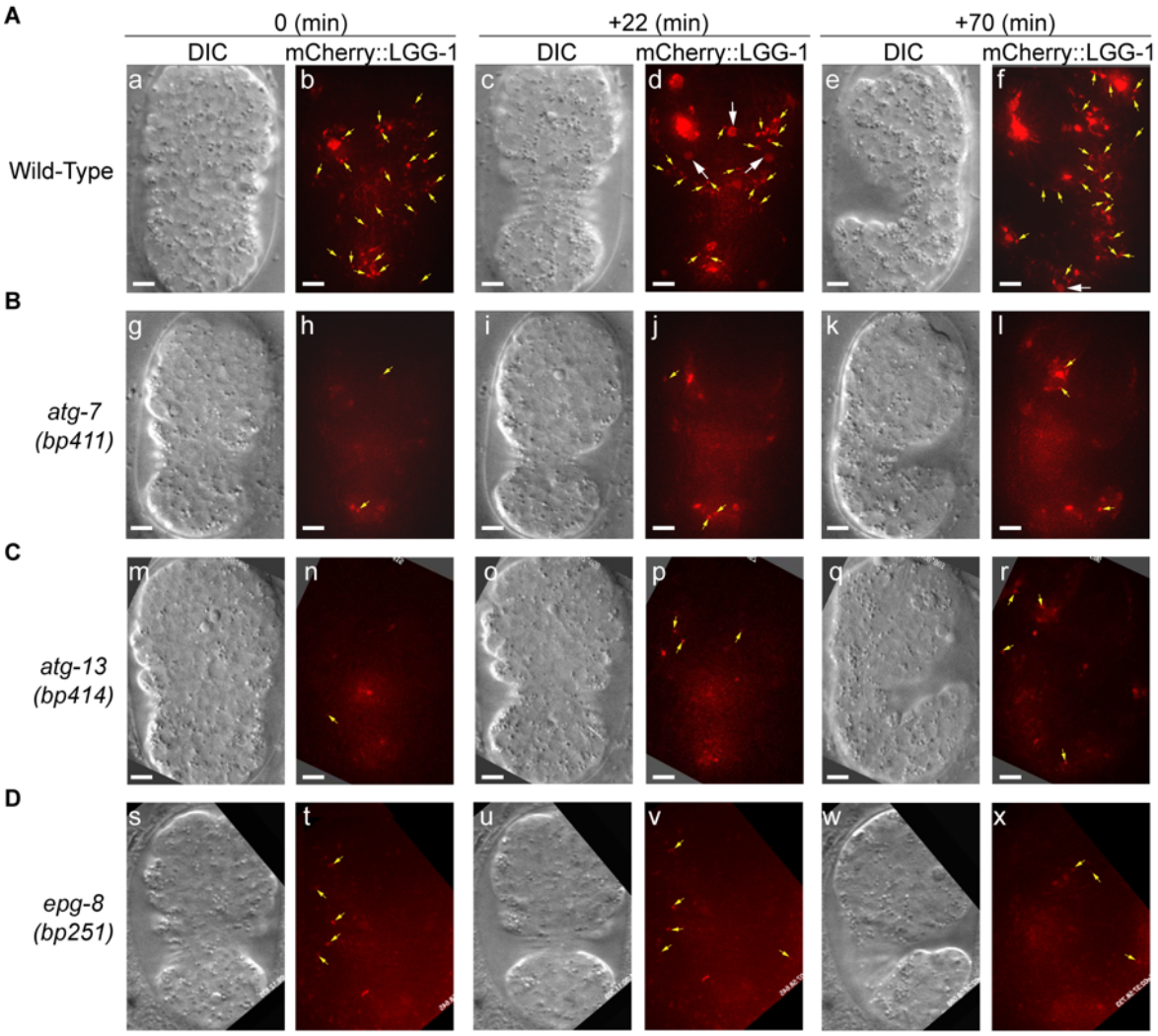

Figure S1. The *atg-7*, *atg-13*, and *epg-8* mutants are severely defective in the production of LGG-1-labeled autophagosomes

Images of wild-type (A), *atg-7(bp411)* (B), *atg-13(bp414)* (C), and *epg-8(bp251)* mutant (D) embryos expressing P_{ced-1} *mCherry::lgg-1* are presented. "0 min" labels embryos that are ~330 min post-1st cleavage. The mCherry images are 2-D projections of 14 Z-sections at 0.5 μm intervals. Red puncta (yellow arrows) represent autophagosomes. White arrows in (A(d)) mark three phagosomes, on the surface of which mCherry signal is recruited in (a-b), and 20 min later, enters the phagosome, demonstrating the autophagosomes/phagosome fusion event. Scale bars are 5 μm.

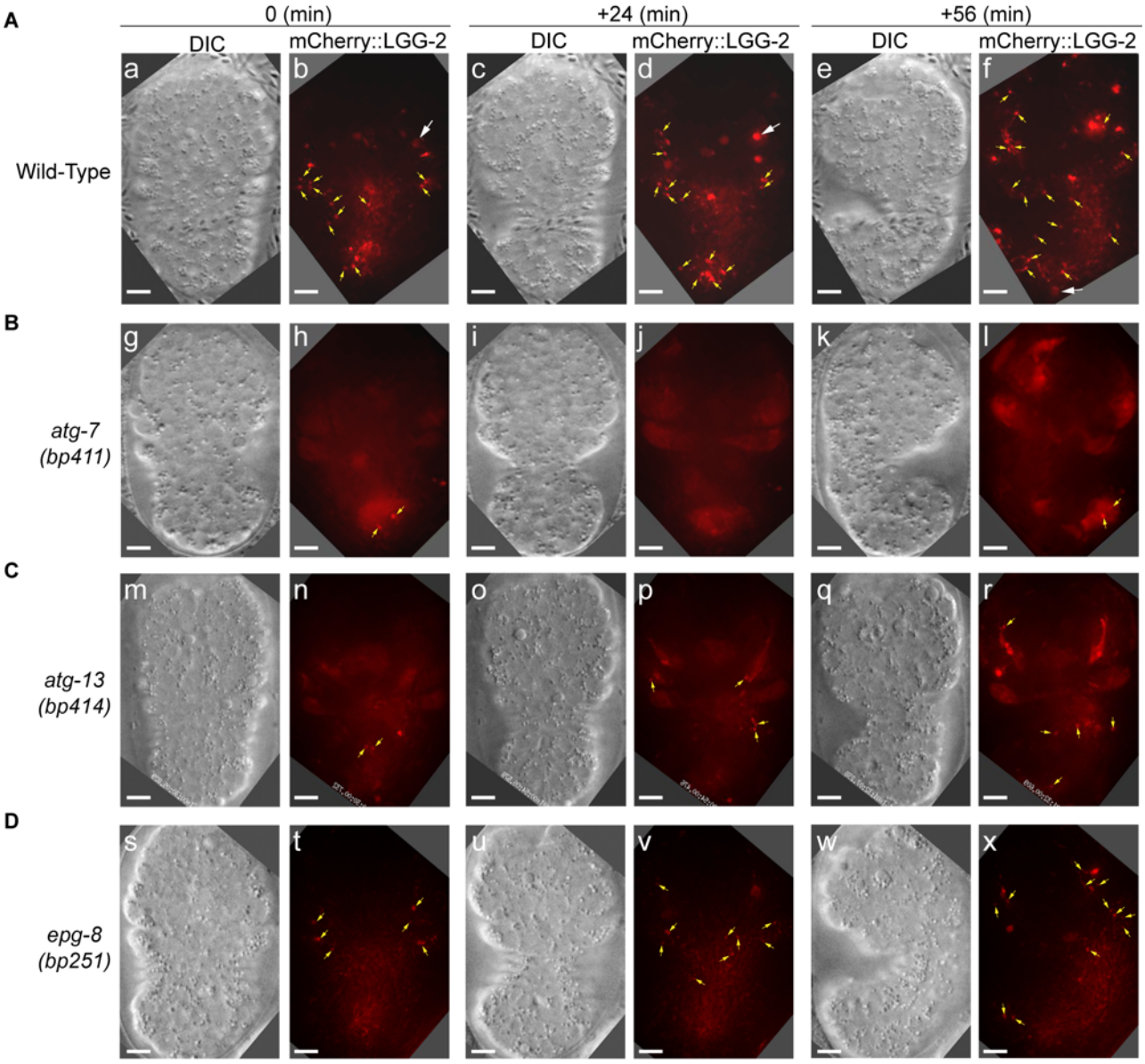

Figure S2. The *atg-7*, *atg-13*, and *epg-8* mutants are severely defective in the production of LGG-2-labeled autophagosomes

Images of wild-type (A), *atg-7(bp411)* (B), *atg-13(bp414)* (C), and *epg-8(bp251)* mutant (D) embryos expressing $P_{ced\text{-}1}$ *mCherry::lgg-1* are presented. "0 min" labels embryos that are ~330 min post-1st cleavage. The mCherry images are 2-D projections of 14 Z-sections at 0.5 μm intervals. Red puncta (yellow arrows) represent autophagosomes. White arrows in (A(b, d)) mark one phagosome, on the surface of which mCherry puncta are recruited to in (b), and 24 min later, mCherry enters the phagosome, demonstrating the autophagosomes/phagosome fusion event. Scale bars are 5 μm.

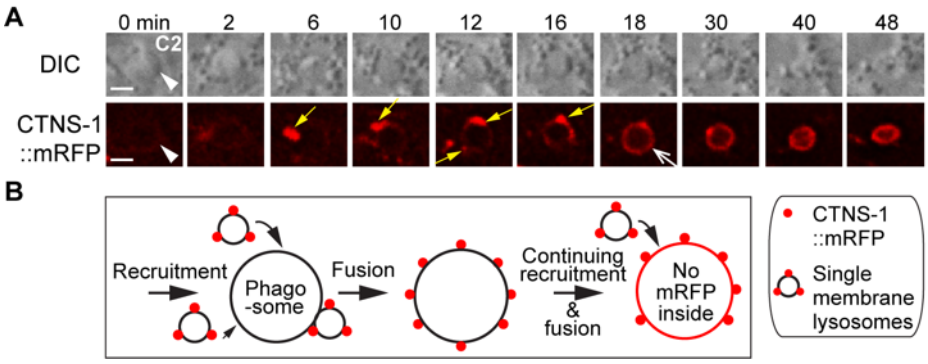

Figure S3. The fusion of lysosomal particles to phagosomes results in the incorporation of lysosomal membrane protein CTNS-1 to the phagosomal membrane but not the lumen

(A) Time-lapse images of a C2 phagosome and the lysosomes that are recruited to and subsequently fuse with it. CTNS-1::mRFP is expressed in engulfing cells under P_{ced-1}. "0 in" is the time point when a C2 phagosome (white arrowheads) just forms. Yellow arrows mark CTNS-1::mRFP-labeled lysosomal particles. One open white arrow marks the phagosomal surface that is evenly colored by mRFP. Scale bars are 2μm.

(B) A diagram illustrating that the single membrane-vesicles that are labeled with CTNS-1::mRFP on their membranes are recruited to phagosomal surfaces and fused to the phagosomal membrane. After the fusion between the membranes of these vesicles and the phagosome, the mRFP signal is evenly distributed to the phagosomal surface. However, no mRFP signal enters the phagosomal lumen.

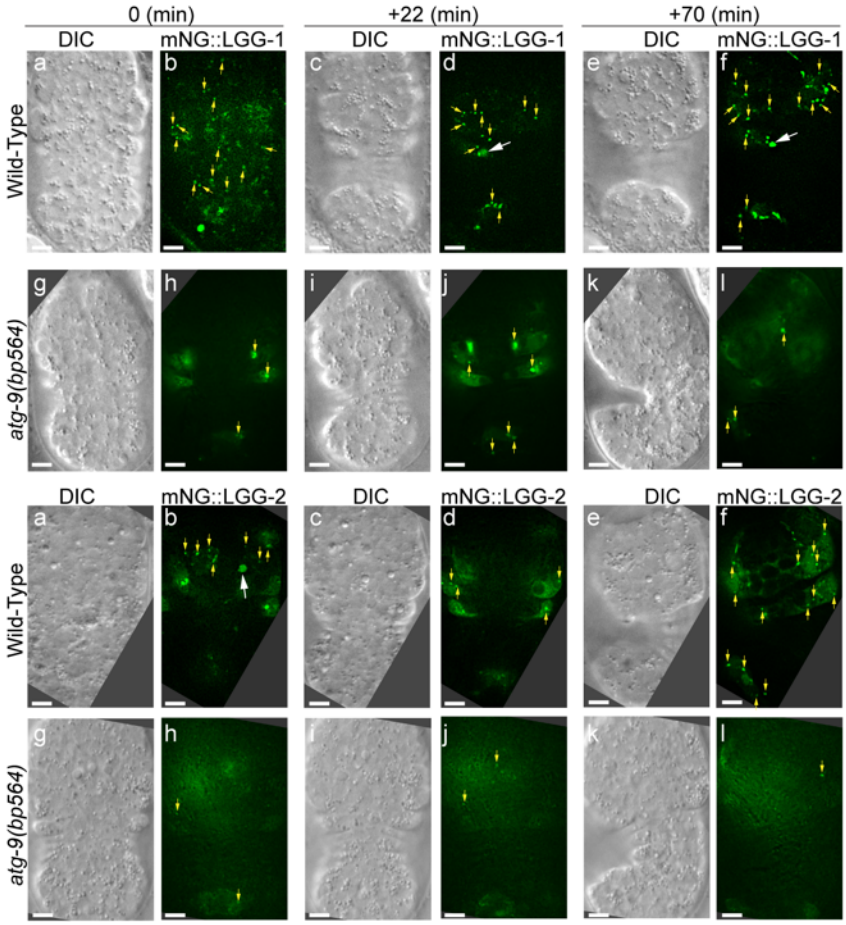

Figure S4. *atg-9* is another gene essential for the production of autophagosomes and the incorporation of autophagosomes into phagosomes

(A-B) Time-lapse image series monitoring the presence or absence of puncta labeled with mNG:: LGG-1 (A) or mNG::LGG-2 (B) on phagosomes (white arrowheads) and the subsequent entry of mCherry signal into the lumen in *atg-7* mutant embryos. DIC images mark the position of the cell corpse. "0 min": when engulfment is just completed (determined by PH::mCherry). Scale bars are 2μm. Yellow arrows mark mNG puncta located on the surfaces of phagosomes.

(C-D) Box-and-Whiskers plots of the relative mNG signal intensity measured in the center of phagosomes 60 min-post the formation of nascent C3 phagosomes from 15 each of wild-type and *atg-9(bp564)* mutant embryos.

(E-F) Images of wild-type and *atg-9(bp564)* mutant embryos expressing $P_{ced\text{-}1}$ *mNG::lgg-1* (E) or *::lgg-2* (F) are presented. "0 min" embryos are embryos at ~330 min post-1st cleavage. The mNG images are 2-D projections of 14 Z-sections at 0.5 μm intervals each. Green puncta (yellow arrows) represent autophagosomes. White arrows in (E(d, f)) and F(b) mark phagosomes in which mNG signal was detected, indicating the existence of autophagosomes/phagosome fusion events. Scale bars are 5 μm.

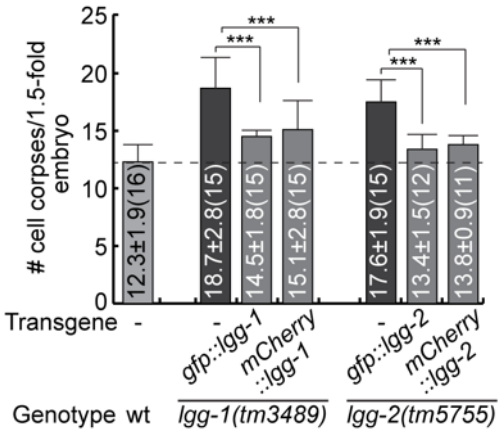

Figure S5. The expression of *lgg-1* and *lgg-2* cDNA in engulfing cells suppresses the Ced phenotype of *lgg-1* and *lgg-2* null mutants, respectively.

GFP- and mCherry-tagged reporters for LGG-1 and LGG-2 are expressed in engulfing cells under the control of the P_{ced-1} promoter in *lgg-1(tm3489)* and *lgg-2(tm5755)* mutant embryos, respectively. The bar graph displays the average number of somatic cell corpses in *lgg-1(tm3489)* and *lgg-2(tm5755)* mutant embryos at the 1.5-fold stage, both with and without the expression of the rescuing construct. The number of embryos scored for each strain is in parentheses. Bars represent the mean, and the error bars indicate standard deviation. Brackets above the bars indicate the samples that are compared by the Student *t*-test. *p*-values are summarized as such: *, $0.001 < p < 0.05$; **, $0.0001 < p < 0.001$; ***, $p < 0.0001$; ns, no significant difference.

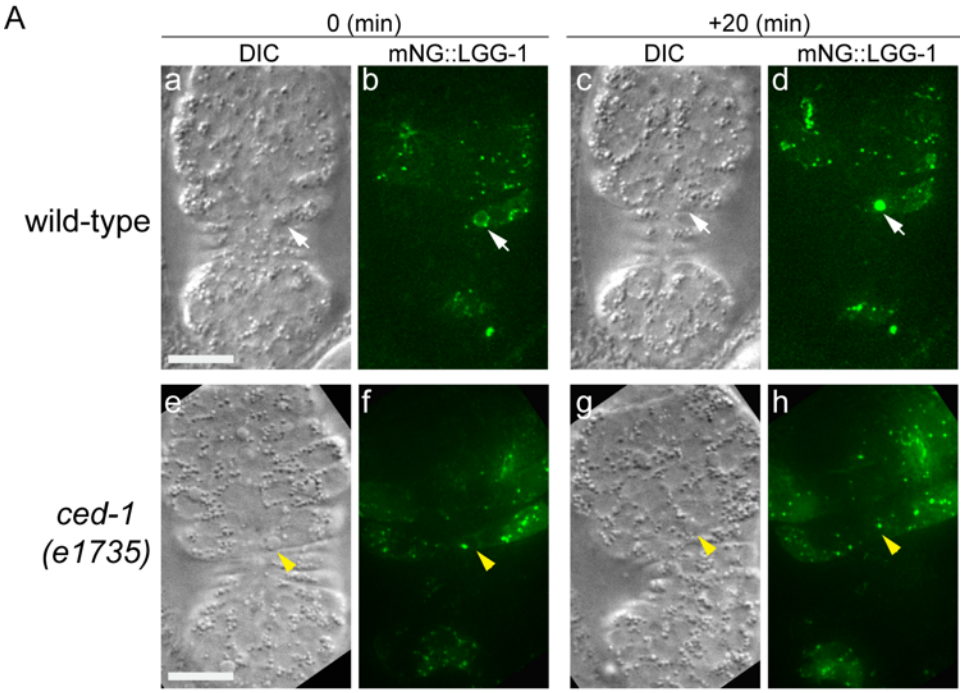

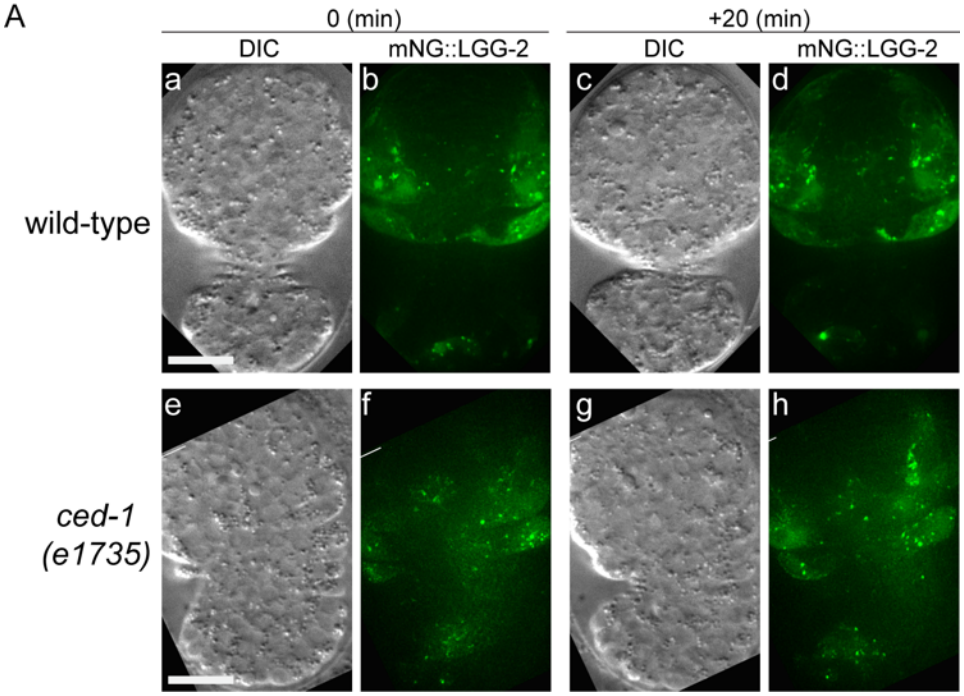

Figure S6. The generation of autophagosomes is normal in *ced-1* mutants.
Images of wild-type and *ced-1(e1735)* mutant embryos expressing P_{ced-1} *mNG::lgg-1* (A) or P_{ced-1}*lgg-2::mNG* (B) are presented. (a-b and e-f) Embryos are at ~370 min post-1st cleavage; (c-d and g-h) Embryos 20 min later. (a, c, e, g) DIC images. (b, d, f, h) 2-D projection of 14 consecutive Z-sections at 0.5 μm interval each. Green puncta represent autophagosomes. White arrows in (A(a-d)) marks one C3 phagosome, onto which LGG-1::mNG puncta are recruited in (a-b); 20 min later (c-d), LGG-1::mNG enters this phagosome, showing an autophagosomes/phagosome fusion event. Yellow arrowheads in (A(e-h)) marks one C3 phagosome on the

surface, of which only one mNG punctum was found (f), and no mNG signal enters the phagosome (h), indicating the lack of recruitment and fusion. Scale bars are 10 μm.

Table S1.

Reagent Type (species) or resource	Designation	Source or Reference	Identifiers	Additional information
Strain, strain background *(E. coli)*	OP50	CGC	ID_ZZhouDatabase:OP50	OP50
Strain, strain background *(C. elegans)*	N2	CGC	ID_ZZhouDatabase:N2	Wild-type Bristol N2
Strain, strain background *(C. elegans)*	CB911	CGC	ID_ZZhouDatabase:CB911	*unc-76(e911)*
Strain, strain background *(C. elegans)*	MT9011	Barbara Conradt	ID_ZZhouDatabase:MT9011	*ced-1(e1735) I ; unc-76(e911) V*
Strain, strain background *(C. elegans)*	ZH2916	This study	ID_ZZhouDatabase:ZH2916	*ced-1(e1735) I ; unc-76(e911) V ; enEx1470 (Injection mix: pOPR007(Pced-1 mNG::lgg-1) 5ng/ul + pUNC-76(+) 20ng/ul + pNL9(Pced-1 PH::mrfp) 5ng/ul)*
Strain, strain background *(C. elegans)*	ZH2934	This study	ID_ZZhouDatabase:ZH2934	*ced-1(e1735) I ; unc-76(e911) V enIs85 V*
Strain, strain background *(C. elegans)*	HZ1691	CGC	ID_ZZhouDatabase:HZ1691	*epg-8(bp251) I ; him-5(1490) V*
Strain, strain background *(C. elegans)*	ZH2954	This study	ID_ZZhouDatabase:ZH2954	*epg-8(bp251) I ; enIs82 II ; unc-76(e911) V*

Strain, strain background *(C. elegans)*	ZH2955	This study	ID_ZZhouDatabase:ZH2955	*epg-8(bp251) I ; unc-76(e911) him-5(1490) V ; enIs83 X*
Strain, strain background *(C. elegans)*	ZH3088	This study	ID_ZZhouDatabase:ZH3088	*epg-8(bp251) I ; unc-76(e911) enIs36 V*
Strain, strain background *(C. elegans)*	ZH2891	This study	ID_ZZhouDatabase:ZH2891	*unc-76(e911) V ; enEx1461 (injection mix pUNC-76 20ng/ul, (pNL9)PH::mRFP 5ng/ul, (pOPR007)Pced-1 mNG::lgg-1 5ng/ul)*
Strain, strain background *(C. elegans)*	ZH2992	This study	ID_ZZhouDatabase:ZH2992	*enIs87 I ; unc-76(e911) V This is an integrant from the ZH2891 background.*
Strain, strain background *(C. elegans)*	GK738	National Bioscience Project of Japan	ID_ZZhouDatabase:GK738	*lgg-1(tm3489) II / mIn1 II*
Strain, strain background *(C. elegans)*	ZH2380	This study	ID_ZZhouDatabase:ZH2380	*lgg-1(tm3489) II / mIn1 II ; unc-76(e911) V*
Strain, strain background *(C. elegans)*	ZH2835	This study	ID_ZZhouDatabase:ZH2835	*lgg-1(tm3489) II / mIn1 II ; unc-76(e911) V enIs36 V*
Strain, strain background *(C. elegans)*	ZH2831	This study	ID_ZZhouDatabase:ZH2831	*lgg-1(tm3489) II / mIn1 II ; lgg-2(tm5755) IV*
Strain, strain background *(C. elegans)*	ZH2838	This study	ID_ZZhouDatabase:ZH2838	*lgg-1(tm3489) II / mIn1 II ; unc-76(e911) V ; enEx1428 (injection mix pUNC-76(+)(20ng/ul), pZZ1052 Pced-1 gfp::Lgg-1 (5ng/ul))*
Strain, strain background *(C. elegans)*	ZH2841	This study	ID_ZZhouDatabase:ZH2841	*lgg-1(tm3489) II / mIn1 II ; unc-76(e911) V ; enEx1431 (injection mix pUNC-76(+)(20ng/ul), pZZ1091 Pced-1 mcherry ::Lgg-1 (5ng/ul))*

Strain, strain background *(C. elegans)*	VC308	CGC	ID_ZZhouDatabase:VC308	*rab-7 (ok511) II / mIn1 II*
Strain, strain background *(C. elegans)*	ZH732	Z.Zhou Lab	ID_ZZhouDatabase:ZH732	*rab-7 (ok511) II / mIn1 II ; unc-76(e911) V*
Strain, strain background *(C. elegans)*	ZH2782	This study	ID_ZZhouDatabase:ZH2782	*rab-7 (ok511) II / mIn1 II ; unc-76(e911) V ; enEx1376 (Injection mix pUNC-76(+)(20ng/ul), pZZ1091 (Pced-1 mcherry::Lgg-1)(5ng/ul))*
Strain, strain background *(C. elegans)*	ZH2715	This study	ID_ZZhouDatabase:ZH2715	*rab-7 (ok511) II / mIn1 II ; unc-76(e911) V ; enEx1320 I (Injection mix pUNC-76(+)(20ng/ul), pXL89(Pced-1mcherry23aa::lgg-2)(5ng/ul))*
Strain, strain background *(C. elegans*	FX01125	National Bioscience Project of Japan	ID_ZZhouDatabase:FX01125	*vps-18/W06B4.3(tm1125) II*
Strain, strain background *(C. elegans)*	ZH2929	This study	ID_ZZhouDatabase:ZH2929	*vps-18/W06B4.3(tm1125) II ; unc-76(e911) V ; enIs83 X*
Strain, strain background *(C. elegans)*	ZH2907	This study	ID_ZZhouDatabase:ZH2907	*vps-18/W06B4.3(tm1125) II ; unc-76(e911) V ; enIs80 V*
Strain, strain background *(C. elegans)*	ZH2734	This study	ID_ZZhouDatabase:ZH2734	*Injected into CB911 with pUNC-76(+)(20ng/ul), pZZ985(Pced-1 ced-1::gfp) (5ng/ml),pZZ1091(Pced-1mcherry::Lgg-1)(5ng/ul)*
Strain, strain background *(C. elegans)*	ZH2919	This study	ID_ZZhouDatabase:ZH2919	*enIs82 II ; unc-76(e911) V (This is an integrant from the ZH2734 background.)*
Strain, strain background *(C. elegans)*	HZ1688	CGC	ID_ZZhouDatabase:HZ1688	*atg-13(bp414) III*
Strain, strain background *(C. elegans)*	ZH2952	This study	ID_ZZhouDatabase:ZH2952	*enIs82 II ; atg-13(bp414) III*

Strain, strain background *(C. elegans)*	ZH2953	This study	ID_ZZhouDatabase:ZH2953	*atg-13(bp414) III ; enIs83 X*
Strain, strain background *(C. elegans)*	ZH3087	This study	ID_ZZhouDatabase:ZH3087	*atg-13(bp414) III ; enIs36 V unc-76(e911) V*
Strain, strain background *(C. elegans)*	MT4970	CGC	ID_ZZhouDatabase:MT4970	*ced-6(n2095) III*
Strain, strain background *(C. elegans)*	MT10539	Z.Zhou Lab	ID_ZZhouDatabase:MT10539	*ced-6(n2095) III ; unc-76(e911) V*
Strain, strain background *(C. elegans)*	ZH2994	This study	ID_ZZhouDatabase:ZH2994	*enIs82 II ; ced-6(n2095) III ; unc-76(e911) V*
Strain, strain background *(C. elegans)*	ZH2995	This study	ID_ZZhouDatabase:ZH2995	*ced-6(n2095) III ; unc-76(e911) V ; enIs83 X*
Strain, strain background *(C. elegans)*	HZ1684	CGC	ID_ZZhouDatabase:HZ1684	*atg-3(bp412) IV ; him-5(e1490) V*
Strain, strain background *(C. elegans)*	ZH2939	This study	ID_ZZhouDatabase:ZH2939	*atg-3(bp412) IV ; enIs85 V unc-76(e911) V*
Strain, strain background *(C. elegans)*	ZH2956	This study	ID_ZZhouDatabase:ZH2956	*atg-3(bp412) IV ; enIs83 X*
Strain, strain background *(C. elegans)*	HZ1686	CGC	ID_ZZhouDatabase:HZ1686	*bnIs1 I ; atg-7(bp411) IV ; him-5(e1490) V*
Strain, strain background *(C. elegans)*	ZH2950	This study	ID_ZZhouDatabase:ZH2950	*enIs82 II ; atg-7(bp411) IV ; unc-76(e911) V*

Strain, strain background *(C. elegans)*	ZH2951	This study	ID_ZZhouDatabase:ZH2951	*atg-7(bp411) IV ; enIs83 X*
Strain, strain background *(C. elegans)*	MT8791	Z.Zhou Lab	ID_ZZhouDatabase:MT8791	*ced-5(n1812) IV ; unc-76(e911) V*
Strain, strain background *(C. elegans)*	ZH3009	This study	ID_ZZhouDatabase:ZH3009	*ced-5(n1812) IV ; unc-76(e911) V ; enIs83 X*
Strain, strain background *(C. elegans)*	ZH3010	This study	ID_ZZhouDatabase:ZH3010	*enIs82 II ; ced-5(n1812) IV ; unc-76(e911) V*
Strain, strain background *(C. elegans)*	MT9288	Z.Zhou Lab	ID_ZZhouDatabase:MT9288	*ced-10(n1993) IV ; unc-76(e911) V*
Strain, strain background *(C. elegans)*	ZH3011	This study	ID_ZZhouDatabase:ZH3011	*enIs82 II ; ced-10(n1993) IV ; unc-76(e911) V*
Strain, strain background *(C. elegans)*	ZH3012	This study	ID_ZZhouDatabase:ZH3012	*ced-10(n1993) IV ; unc-76(e911) V ; enIs83 X*
Strain, strain background *(C. elegans)*	FX14610	National Bioscience Project of Japan	ID_ZZhouDatabase:FX14610	*lgg-2(tm5755) IV*
Strain, strain background *(C. elegans)*	ZH2517	This study	ID_ZZhouDatabase:ZH2517	*lgg-2(tm5755) IV ; unc-76(e911) V*
Strain, strain background *(C. elegans)*	ZH2632	This study	ID_ZZhouDatabase:ZH2632	*lgg-2(tm5755) IV ; unc-76(e911) V ; enEx1267 (injection mix Punc-76(+) 20ng/ul, pTY02(Pced-1::gfp::lgg2long)5ng/ul)*

Strain, strain background *(C. elegans)*	ZH2573	This study	ID_ZZhouDatabase:ZH2573	*lgg-2(tm5755) IV ; unc-76(e911) V ; enEx1223 (injection mix lgg-2(tm5755); unc-76(e911) injected with pXL89(Pced-1mcherry-23aa::lgg-2, 10ng/ul) + pUNC-76(25ng/ul))*
Strain, strain background *(C. elegans)*	ZH2875	This study	ID_ZZhouDatabase:ZH2875	*lgg-2(tm5755) IV ; unc-76(e911) V enIs36 V*
Strain, strain background *(C. elegans)*	FX06474	CGC	ID_ZZhouDatabase:FX06474	*lgg-2(tm6474) IV*
Strain, strain background *(C. elegans)*	ZH2519	This study	ID_ZZhouDatabase:ZH2519	*lgg-2(tm6474) IV ; unc-76(e911) V*
Strain, strain background *(C. elegans)*	ZH2889	This study	ID_ZZhouDatabase:ZH2889	*unc-76(e911) V ; enEx1459 (injection mix pUNC-76 20ng/ul, (pNL9)PH::mRFP 5ng/ul,(pOPR004)Pced-1 mNG::lgg-2 5ng/ul)*
Strain, strain background *(C. elegans)*	ZH2921	This study	ID_ZZhouDatabase:ZH2921	*enIs85 V unc-76(e911) V This is an integrant from the ZH2889 background.*
Strain, strain background *(C. elegans)*	ZH2734	This study	ID_ZZhouDatabase:ZH2934	*unc-76(e911) V ; enEx1335 (injection mix pUNC-76(+)(20ng/ul), pZZ985(Pced-1 ced-1::gfp) (5ng/ml),pZZ1091(Pced-1mcherry::Lgg-1)(5ng/ul) Line 1.)*
Strain, strain background *(C. elegans)*	ZH2918	This study	ID_ZZhouDatabase:ZH2918	*unc-76(e911) V ; enIs80 IV This is an integrant from the ZH2734 background.*
Strain, strain background *(C. elegans)*	ZH814	Z.Zhou Lab	ID_ZZhouDatabase:ZH814	*unc-76(e911) V ; enEx339 (injection mix pUNC-76 50ng/uL + pZZ610 (Pced-1 ced-1::gfp) 20ng/uL + pIH1 (Pced-1 2xFYVE::mRFP1) 20 ng/uL)*
Strain, strain background *(C. elegans)*	ZH989	Z.Zhou Lab	ID_ZZhouDatabase:ZH989	*unc-76(e911) V enIs36 V This is an integrant from the ZH814 background.*

Strain, strain background *(C. elegans)*	HZ1687	CGC	ID_ZZhouDatabase:HZ1687	*atg-9(bp564) V him-5(e1490) V*
Strain, strain background *(C. elegans)*	ZH2803	This study	ID_ZZhouDatabase:ZH2803	*atg-9(bp564) V him-5(e1490) V ; lin-15AB(n765ts) X*
Strain, strain background *(C. elegans)*	ZH2903	This study	ID_ZZhouDatabase:ZH2903	*atg-9(bp564) V him-5(e1490) V ; lin-15AB(n765ts) X ; enEx1468 (injection mix Lin15(+) 50ng/ul, (pNL9) PH::mRFP 5ng/ul, (pOPR007) Pced-1 mNG::lgg-1 5ng/ul (line1))*
Strain, strain background *(C. elegans)*	ZH2922	This study	ID_ZZhouDatabase:ZH2922	*atg-9(bp564) V him-5(e1490) V ; lin-15AB(n765ts) X ; enEx1472 (injection mix Lin15(+) 50ng/ul, (pNL9) PH::mRFP 10ng/ul, (pOPR004) Pced-1 mNG::lgg-2 10ng/ul (line1))*
Strain, strain background *(C. elegans)*	VC893	CGC	ID_ZZhouDatabase:VC893	*atg-18(gk378) V*
Strain, strain background *(C. elegans)*	ZH2804	This study	ID_ZZhouDatabase:VC893	*atg-18(gk378) V ; lin-15AB(n765ts) X*
Strain, strain background *(C. elegans)*	ZH2902	This study	ID_ZZhouDatabase:ZH2902	*atg-18(gk378) V ; lin-15AB(n765ts) X ; enEx1467 (injection mix Lin15(+) 50ng/ul, (pNL9) PH::mRFP 5ng/ul, (pOPR007) Pced-1 mNG::lgg-1 5ng/ul)*
Strain, strain background *(C. elegans)*	ZH2942	This study	ID_ZZhouDatabase:ZH2902	*atg-18(gk378) V ; lin-15AB(n765ts) X ; enEx1482 (injection mix Lin-15(+) 50ng/ul + pNL9((PH::mRFP) 10ng/ul + pOPR004 (Pced-1 mNG::LGG-2) 10ng/ul)*
Strain, strain background *(C. elegans)*	HZ1683	This study	ID_ZZhouDatabase:HZ1683	*him-5(e1490) V ; atg-2(bp576) X*

Strain, strain background *(C. elegans)*	ZH2345	This study	ID_ZZhouDatabase:ZH2346	*unc-76(e911) V ; atg-2(bp576) X*
Strain, strain background *(C. elegans)*	ZH445	Z.Zhou Lab	ID_ZZhouDatabase:ZH445	*unc-76(e911) V ; dyn-1(n4039) X ; enEx21 (injection mix Pdyn-1 dyn-1 8ng/ul)*
Strain, strain background *(C. elegans)*	ZH3014	This study	ID_ZZhouDatabase:ZH3014	*enIs87 I ; unc-76(e911) V ; dyn-1(n4039) X ; enEx2*
Strain, strain background *(C. elegans)*	ZH3015	This study	ID_ZZhouDatabase:ZH3015	*enIs85 V unc-76(e911) V ; dyn-1(n4039) X ; enEx21*
Strain, strain background *(C. elegans)*	ZH2743	This study	ID_ZZhouDatabase:ZH2743	*unc-76(e911) V ; enEx1348 (injection mix pUNC-76(+)(20ng/ul)+pZZ985,CED-1::GFP(5ng/ul)+pXL89, Pced-1mcherry23aa::Lgg-2 (5ng/ul))*

Supplemental movie legends

Movie S1. mCherry::LGG-1-labeled vesicles are recruited to the surface of a phagosome and subsequently fuse to the phagosome

Related to **Fig 1E**. This movie shows time-lapse recording images of a C3 phagosome (white arrowheads) in a wild-type embryo, starting at ~330 min post-1st cleavage. CED-1::GFP labels pseudopods, allowing the visualization of the phagosome formation process. "0 min" is the moment when pseudopods just seals. Yellow arrowheads indicate the mCherry::LGG-1^{+} puncta, and open white arrows point to the phagosome lumen containing the mCherry signal.

Movie S2. mCherry::LGG-2-labeled vesicles are recruited to the surface of a phagosome and subsequently fuse to the phagosome

Related to **Fig 1H**. This movie shows time-lapse recording images of a C3 phagosome (white arrowheads) in a wild-type embryo, starting at ~330 min post-1st cleavage. CED-1::GFP labels pseudopods, allowing the visualization of the phagosome formation process. "0 min" is the moment when pseudopods just seals. Yellow arrowheads indicate the mCherry::LGG-2^{+} puncta, and open white arrows point to the phagosome lumen containing the mCherry signal.

Movie S3. mNG::LGG-1-labeled vesicles are recruited to the surface of a phagosome and subsequently fuse to the phagosome.
Related to **Fig 1F**. This movie shows time-lapse recording images of a C3 phagosome in a wild-type embryo, starting at ~330 min post-1st cleavage. PH(hPLCγ)::mRFP labels pseudopods, allowing the visualization of the phagosome formation process. "0 min" is the moment when pseudopods just seals. Yellow arrowheads indicate mNG::LGG-1^{+} puncta, and open white arrows point to the phagosome with mNG signal in its lumen.

Movie S4. In *rab-7 (ok511),* mCherry::LGG-1-labeled vesicles fail to fuse with phagosomes.
Related to **Fig 7E**. This movie shows time-lapse recording images of a C3 phagosome in a *rab-7(ok511)* m^{-}z^{-} homozygous embryo, starting at ~330 min post-1st cleavage. "0 min" is the moment when a nascent phagosome is just formed. White arrowheads mark the phagosome. Yellow arrows mark mCherry::LGG-1^{+} puncta.

Movie S5. In *rab-7(ok511)* mutants, mCherry::LGG-2-labeled vesicles fail to fuse with phagosomes.
Related to **Fig 7F**. This movie shows time-lapse recording images of a C3 phagosome in a *rab-7(ok511)* m^{-}z^{-} homozygous embryos, starting at ~330 min post-1st cleavage. "0 min" is the moment when a nascent phagosome is just formed. White arrowheads mark the phagosome. Yellow arrows mark mCherry::LGG-2^{+} puncta.

Movie S6. In *ced-1(e1735)* mutants, mNG::LGG-1-labeled vesicles fail to be recruited to the phagosomal surface.
Related to **Fig 8A**. This movie shows time-lapse recording images of a C3 phagosome in a *ced-1(e1735)* embryo, starting at ~300 min post-1st cleavage. "0 min" is the moment when a nascent phagosome is just formed. White arrowheads mark the phagosome; yellow arrows label mNG::LGG-1^{+} puncta.

References

1. Reddien PW, Horvitz HR (2004) The engulfment process of programmed cell death in caenorhabditis elegans. Annu Rev Cell Dev Biol 20: 193-221.
2. Nagata S (2018) Apoptosis and Clearance of Apoptotic Cells. Annu Rev Immunol.
3. Levin R, Grinstein S, Canton J (2016) The life cycle of phagosomes: formation, maturation, and resolution. Immunol Rev 273: 156-179.
4. Schaaf MB, Keulers TG, Vooijs MA, Rouschop KM (2016) LC3/GABARAP family proteins: autophagy-(un)related functions. FASEB J 30: 3961-3978.
5. Sanjuan MA, Dillon CP, Tait SW, Moshiach S, Dorsey F, et al. (2007) Toll-like receptor signalling in macrophages links the autophagy pathway to phagocytosis. Nature 450: 1253-1257.
6. Green DR, Oguin TH, Martinez J (2016) The clearance of dying cells: table for two. Cell Death Differ 23: 915-926.
7. Martinez J, Almendinger J, Oberst A, Ness R, Dillon CP, et al. (2011) Microtubule-associated protein 1 light chain 3 alpha (LC3)-associated phagocytosis is required for the efficient clearance of dead cells. Proc Natl Acad Sci U S A 108: 17396-17401.
8. Martinez J, Cunha LD, Park S, Yang M, Lu Q, et al. (2016) Noncanonical autophagy inhibits the autoinflammatory, lupus-like response to dying cells. Nature 533: 115-119.
9. Morishita H, Mizushima N (2019) Diverse Cellular Roles of Autophagy. Annu Rev Cell Dev Biol 35: 453-475.
10. Nakatogawa H (2020) Mechanisms governing autophagosome biogenesis. Nat Rev Mol Cell Biol 21: 439-458.
11. Cheng S, Wu Y, Lu Q, Yan J, Zhang H, et al. (2013) Autophagy genes coordinate with the class II PI/PtdIns 3-kinase PIKI-1 to regulate apoptotic cell clearance in C. elegans. Autophagy 9: 2022-2032.
12. Huang S, Jia K, Wang Y, Zhou Z, Levine B (2013) Autophagy genes function in apoptotic cell corpse clearance during C. elegans embryonic development. Autophagy 9: 138-149.
13. Li W, Zou W, Yang Y, Chai Y, Chen B, et al. (2012) Autophagy genes function sequentially to promote apoptotic cell corpse degradation in the engulfing cell. J Cell Biol 197: 27-35.
14. Martinez J, Malireddi RK, Lu Q, Cunha LD, Pelletier S, et al. (2015) Molecular characterization of LC3-associated phagocytosis reveals distinct roles for Rubicon, NOX2 and autophagy proteins. Nat Cell Biol 17: 893-906.
15. Sulston JE, Horvitz HR (1977) Post-embryonic cell lineages of the nematode, Caenorhabditis elegans. Dev Biol 56: 110-156.

16. Sulston JE, Albertson DG, Thomson JN (1980) The Caenorhabditis elegans male: postembryonic development of nongonadal structures. Dev Biol 78: 542-576.
17. Ellis RE, Jacobson DM, Horvitz HR (1991a) Genes required for the engulfment of cell corpses during programmed cell death in Caenorhabditis elegans. Genetics 129: 79-94.
18. Mangahas PM, Zhou Z (2005) Clearance of apoptotic cells in Caenorhabditis elegans. Semin Cell Dev Biol 16: 295-306.
19. Yu X, Lu N, Zhou Z (2008) Phagocytic receptor CED-1 initiates a signaling pathway for degrading engulfed apoptotic cells. PLoS Biol 6: e61.
20. Zhou Z, Hartwieg E, Horvitz HR (2001b) CED-1 is a transmembrane receptor that mediates cell corpse engulfment in C. elegans. Cell 104: 43-56.
21. Yu X, Odera S, Chuang CH, Lu N, Zhou Z (2006) C. elegans Dynamin mediates the signaling of phagocytic receptor CED-1 for the engulfment and degradation of apoptotic cells. Dev Cell 10: 743-757.
22. Shen Q, He B, Lu N, Conradt B, Grant BD, et al. (2013) Phagocytic receptor signaling regulates clathrin and epsin-mediated cytoskeletal remodeling during apoptotic cell engulfment in C. elegans. Development 140: 3230-3243.
23. Lu N, Shen Q, Mahoney TR, Neukomm LJ, Wang Y, et al. (2012) Two PI 3-kinases and one PI 3-phosphatase together establish the cyclic waves of phagosomal PtdIns(3)P critical for the degradation of apoptotic cells. PLoS Biol 10: e1001245.
24. Lu N, Shen Q, Mahoney TR, Liu X, Zhou Z (2011) Three sorting nexins drive the degradation of apoptotic cells in response to PtdIns(3)P signaling. Mol Biol Cell 22: 354-374.
25. Lu N, Zhou Z (2012) Membrane trafficking and phagosome maturation during the clearance of apoptotic cells. Int Rev Cell Mol Biol 293: 269-309.
26. Manil-Segalen M, Lefebvre C, Jenzer C, Trichet M, Boulogne C, et al. (2014) The C. elegans LC3 acts downstream of GABARAP to degrade autophagosomes by interacting with the HOPS subunit VPS39. Dev Cell 28: 43-55.
27. Lu N, Yu X, He X, Zhou Z (2009) Detecting apoptotic cells and monitoring their clearance in the nematode Caenorhabditis elegans. Methods Mol Biol 559: 357-370.
28. Wu F, Watanabe Y, Guo XY, Qi X, Wang P, et al. (2015) Structural Basis of the Differential Function of the Two C. elegans Atg8 Homologs, LGG-1 and LGG-2, in Autophagy. Mol Cell 60: 914-929.
29. Tsien RY (1998) The green fluorescent protein. Annu Rev Biochem 67: 509-544.

30. Shaner NC, Campbell RE, Steinbach PA, Giepmans BN, Palmer AE, et al. (2004) Improved monomeric red, orange and yellow fluorescent proteins derived from Discosoma sp. red fluorescent protein. Nat Biotechnol 22: 1567-1572.
31. Shinoda H, Ma Y, Nakashima R, Sakurai K, Matsuda T, et al. (2018) Acid-Tolerant Monomeric GFP from Olindias formosa. Cell Chem Biol 25: 330-338 e337.
32. Tian Y, Li Z, Hu W, Ren H, Tian E, et al. (2010) C. elegans screen identifies autophagy genes specific to multicellular organisms. Cell 141: 1042-1055.
33. Yang P, Zhang H (2011) The coiled-coil domain protein EPG-8 plays an essential role in the autophagy pathway in C. elegans. Autophagy 7: 159-165.
34. Zhang H, Baehrecke EH (2015) Eaten alive: novel insights into autophagy from multicellular model systems. Trends Cell Biol.
35. Gomes LC, Odedra D, Dikic I, Pohl C (2016) Autophagy and modular restructuring of metabolism control germline tumor differentiation and proliferation in C. elegans. Autophagy 12: 529-546.
36. Lin L, Yang P, Huang X, Zhang H, Lu Q, et al. (2013) The scaffold protein EPG-7 links cargo-receptor complexes with the autophagic assembly machinery. J Cell Biol 201: 113-129.
37. Lu Q, Yang P, Huang X, Hu W, Guo B, et al. (2011) The WD40 repeat PtdIns(3)P-binding protein EPG-6 regulates progression of omegasomes to autophagosomes. Dev Cell 21: 343-357.
38. Wu F, Wang P, Shen Y, Noda NN, Zhang H (2016) Small differences make a big impact: Structural insights into the differential function of the 2 Atg8 homologs in C. elegans. Autophagy 12: 606-607.
39. Balderhaar HJ, Ungermann C (2013) CORVET and HOPS tethering complexes - coordinators of endosome and lysosome fusion. J Cell Sci 126: 1307-1316.
40. Szatmari Z, Sass M (2014) The autophagic roles of Rab small GTPases and their upstream regulators: a review. Autophagy 10: 1154-1166.
41. McEwan DG, Popovic D, Gubas A, Terawaki S, Suzuki H, et al. (2015) PLEKHM1 regulates autophagosome-lysosome fusion through HOPS complex and LC3/GABARAP proteins. Mol Cell 57: 39-54.
42. Xiao H, Chen D, Fang Z, Xu J, Sun X, et al. (2009) Lysosome biogenesis mediated by vps-18 affects apoptotic cell degradation in Caenorhabditis elegans. Mol Biol Cell 20: 21-32.
43. Wu YC, Stanfield GM, Horvitz HR (2000) NUC-1, a caenorhabditis elegans DNase II homolog, functions in an intermediate step of DNA degradation during apoptosis. Genes Dev 14: 536-548.

44. Guo P, Hu T, Zhang J, Jiang S, Wang X (2010) Sequential action of Caenorhabditis elegans Rab GTPases regulates phagolysosome formation during apoptotic cell degradation. Proc Natl Acad Sci U S A 107: 18016-18021.

45. Qu X, Zou Z, Sun Q, Luby-Phelps K, Cheng P, et al. (2007) Autophagy gene-dependent clearance of apoptotic cells during embryonic development. Cell 128: 931-946.

46. Jenzer C, Simionato E, Largeau C, Scarcelli V, Lefebvre C, et al. (2019) Autophagy mediates phosphatidylserine exposure and phagosome degradation during apoptosis through specific functions of GABARAP/LGG-1 and LC3/LGG-2. Autophagy 15: 228-241.

47. Fazeli G, Stetter M, Lisack JN, Wehman AM (2018) C. elegans Blastomeres Clear the Corpse of the Second Polar Body by LC3-Associated Phagocytosis. Cell Rep 23: 2070-2082.

48. Fazeli G, Trinkwalder M, Irmisch L, Wehman AM (2016) C. elegans midbodies are released, phagocytosed and undergo LC3-dependent degradation independent of macroautophagy. J Cell Sci 129: 3721-3731.

49. Vieira OV, Botelho RJ, Grinstein S (2002) Phagosome maturation: aging gracefully. Biochem J 366: 689-704.

50. Spang A (2016) Membrane Tethering Complexes in the Endosomal System. Front Cell Dev Biol 4: 35.

51. Kinchen JM, Doukoumetzidis K, Almendinger J, Stergiou L, Tosello-Trampont A, et al. (2008) A pathway for phagosome maturation during engulfment of apoptotic cells. Nat Cell Biol 10: 556-566.

52. Jiang P, Nishimura T, Sakamaki Y, Itakura E, Hatta T, et al. (2014) The HOPS complex mediates autophagosome-lysosome fusion through interaction with syntaxin 17. Mol Biol Cell 25: 1327-1337.

53. Takáts S, Pircs K, Nagy P, Varga Á, Kárpáti M, et al. (2014) Interaction of the HOPS complex with Syntaxin 17 mediates autophagosome clearance in Drosophila. Mol Biol Cell 25: 1338-1354.

54. Stroupe C, Collins KM, Fratti RA, Wickner W (2006) Purification of active HOPS complex reveals its affinities for phosphoinositides and the SNARE Vam7p. EMBO J 25: 1579-1589.

55. Jeschke A, Haas A (2018) Sequential actions of phosphatidylinositol phosphates regulate phagosome-lysosome fusion. Mol Biol Cell 29: 452-465.

56. Wood WB, Researchers tCo*Ce* (1988) The Nematode *Caenorhabditis elegans*. Cold Spring Harbor, NY: Cold Spring Harbor Laboratory.

57. Riddle DL, Blumenthal T, Meyer BJ, Priess JR, editors (1997) C. elegans II. Plainview, NY: Cold Spring harbor Laboratory Press.

58. Edgley ML, Baillie DL, Riddle DL, Rose AM (2006) Genetic balancers. WormBook: 1-32.

59. Bloom L, Horvitz HR (1997) The Caenorhabditis elegans gene unc-76 and its human homologs define a new gene family involved in axonal outgrowth and fasciculation. Proc Natl Acad Sci U S A 94: 3414-3419.
60. Jin Y (1999) Transformation. In: Hope IA, editor. C elegans, a practical approach. Oxford: Oxford University Press. pp. 69-96.
61. Haley R, Wang Y, Zhou Z (2018) The small GTPase RAB-35 defines a third pathway that is required for the recognition and degradation of apoptotic cells. PLoS Genet 14: e1007558.
62. Shaner NC, Lambert GG, Chammas A, Ni Y, Cranfill PJ, et al. (2013) A bright monomeric green fluorescent protein derived from Branchiostoma lanceolatum. Nat Methods 10: 407-409.